UCRL-1756

UNCLASSIFIED

UNIVERSITY OF CALIFORNIA — BERKELEY

RADIATION LABORATORY

DISCLAIMER

UCRL-1756
Unclassified-Physics Distribution

UNIVERSITY OF CALIFORNIA

Radiation Laboratory

Contract No. W-7405-eng-48

THE EXCITATION FUNCTION FOR π^+-MESONS PRODUCED IN P-P COLLISIONS AT 0° TO THE BEAM

Alvin George Schulz, Jr.
(Thesis)

May 22, 1952

Berkeley, California

TABLE OF CONTENTS

I ABSTRACT

The differential cross sections at one angle for the reaction $p+p \longrightarrow \pi^+ + d$ have been measured as a function of proton energy in the energy range 310 Mev to 336 Mev. Using the external beam of the Berkeley synchrocyclotron, the positive pions produced at $0^\circ \pm 3^\circ$ to the beam direction were magnetically separated from the proton beam, and were detected by scintillation counters using a delayed coincidence between a π^+ meson and its μ^+ decay. A polyethylene-carbon difference was used to obtain the hydrogen contribution. In order to obtain protons at energies below 340 Mev, lead absorbers were placed in the proton beam immediately ahead of the target. The pion yield from the lead was automatically subtracted with the carbon contribution. At each proton energy the positive pion energy spectrum was scanned in the region of the characteristic peak due to the reaction given above. The relative $d\sigma/d\Omega$ was obtained by integrating over meson energy. The results are presented in the following table:

Differential Cross Sections
In Laboratory and Center of Mass Systems

Laboratory		Center of Mass System	
E_{proton} Mev	$\frac{d\sigma}{d\Omega}(0^\circ)$ 10^{-30} cm^2 sterad^{-1}	E_{pion} Mev	$\frac{d\sigma}{d\Omega}(0^\circ)$ 10^{-30} cm^2 sterad^{-1}
336	121 ± 9	19.5	31.3 ± 2.3
330	103 ± 8	17.1	25.8 ± 2.0
325	90 ± 10	14.6	21.6 ± 2.4
321	83 ± 10	12.9	18.7 ± 2.0
315	68 ± 8	10.4	14.2 ± 1.7
311	54 ± 7	8.6	10.3 ± 1.3

The relation of the excitation function to the theoretical analysis of Chew, Goldberger, Steinberger, and Yang is discussed. The relative values have the standard deviations indicated in the table. The absolute value has a standard deviation of 25 per cent.

II. INTRODUCTION

A fundamental problem in meson physics is the production of pions in collisions of free nucleons. The present work is concerned with the excitation function for a particular reaction of this type, namely,

$$p + p \rightarrow \pi^+ + d \qquad (1)$$

The existence of this reaction was first suggested by the early work of a group at Berkeley, headed by Professors C. Richman and H. Wilcox.[1] Using nuclear emulsion detectors embedded in absorbers, and magnetic separation to sort out the mesons formed in the beam direction, they observed the energy spectrum of positive pions from p-p collisions. An intense peak was found near the upper limit allowed by energy considerations. It was thought that this peak might be due to reaction (1) and that the mesons found at lower energies were due to the reaction,

$$p + p \rightarrow \pi^+ + p + n \qquad (2)$$

The first reaction would yield a line spectrum about 4 Mev higher in energy in the laboratory system than the upper energy limit of the continuum expected from the second reaction. The extra energy results from the binding energy released when the deuteron is formed. Subsequently, the existence of reaction (1) was confirmed by Crawford, Crowe, and Stevenson[2] with counters by direct observation of the positive pion and the deuteron in coincidence.

Continued work on the p-p positive pion yield[3,4] pointed to the following conclusions:

1. At zero degrees to the beam, about 70 per cent of the yield was associated with reaction (1).

2. The pions associated with this reaction have an angular distribution in the center of mass frame which is predominantly $\cos^2\theta$, where θ is the angle between the pion and the original beam direction. Detailed examination of the pion peak energy, combined with accurate measurements of the proton beam energy, yielded a positive pion mass in good agreement with that obtained by other methods.[3a].

It was suggested by Marshak[5,6] and others that measurements on the inverse reaction,

$$\pi^+ + d \rightarrow p + p \qquad (3)$$

in conjunction with detailed balancing calculations and the data on reaction (1) could be used to determine the spin of the positive pion. A study of reaction (3) was undertaken by groups at Columbia[7] and Rochester[8]. The results in both cases indicated that the spin is zero, and that the angular distribution of the Columbia group was qualitatively in agreement with that obtained by the Berkeley group.

The angular distribution for reaction (3) was obtained at three pion energies. This excitation data for reaction (3) can be converted to an excitation function for reaction (1) by detailed balancing. The pion energies used for the study of reaction (3) corresponded to proton energies between 345 Mev and 380 Mev in reaction (1).

The excitation function for the reaction $p + p \longrightarrow \pi^+ + d$ in the proton energy region between 310 Mev and 340 Mev has been studied in this experiment. The differential cross sections were measured at $0^\circ \pm 3^\circ$ to the proton beam direction. The threshold for the reaction is 291 Mev. Section III of this report gives a general description of the method employed in the

experiment. Sections IV and V relate details of the experimental techniques and of the method of analysis of the data.

Results of the experiment are contained in Section VI. Graphs of the experimental data are given and the results are compared with those of Durbin, Loar, and Steinberger[9] for higher energies obtained from the inverse reaction by the method of detailed balancing. Finally, the relation between the results obtained and the phenomenological theory of Chew, et al.,[10] is discussed.

III. GENERAL DESCRIPTION OF THE EXPERIMENT

A collimated beam of 340 Mev protons was sent through an ionization chamber whose collected charge was proportional to the integrated proton flux. The beam then impinged on meson production targets placed in a magnetic field. See Fig. 1. Emerging from the target, the proton beam trajectory proceeded through the field region with a small curvature. The positive pions produced in the forward direction turned with a greater curvature than the protons and entered a channel defined by brass shielding. After turning through about 75°, the mesons of interest went through copper absorbers of such a thickness that they stopped in the last crystal of a three-crystal scintillation telescope. The pions were detected by a delayed coincidence between the decay muon in the last crystal and the positive pion passing through the first two crystals.

The production of the pions was studied by means of the usual carbon-polyethylene subtraction technique. The polyethylene and carbon targets were designed to contain the same number of grams per square centimeter of carbon. The difference was taken to be the hydrogen contribution. When it was desired to decrease the proton energy to measure the excitation function for the process being studied, lead absorbers were placed in the proton beam immediately ahead of the production targets. The small contribution of pions coming from the lead was automatically subtracted with the carbon. At each proton energy the positive pion spectrum was scanned in the region of the peak which is due to the reaction $p + p \longrightarrow \pi^{+} + d$. The spectra from polyethylene and carbon were then integrated over meson energy, and the difference was taken to be the differential cross section per unit solid angle for this reaction.

IV. DETAILS OF THE EXPERIMENT

A. Source of Protons and Collimation

The scattered external proton beam of the 184-inch Berkeley synchrocyclotron was used for this experiment. The scattered beam has about a 20-microsecond duration with a repetition rate of 60 cycles per second. The electrostatically deflected beam provides a much greater flux of particles but has a much shorter duty cycle. The scattered beam was chosen because it had an adequate flux of particles and because it had a larger duty cycle. The number of accidental coincidences is inversely proportional to the duty cycle of the beam when using coincidence telescopes.

A small steering magnet located inside the main cyclotron shielding was used to deflect the beam through the main shielding into a secondary shielded area, called the "cave", as shown in Fig. 1. The beam was roughly collimated by a pre-collimator located ahead of the steering magnet. In this way much of the collimation was done where the spray of neutrons and charged particles, introduced by the slits, did not reach the cave. The final collimation was done by means of a 48-inch brass tube located at the point where the beam entered the cave. The resultant beam was contained in a three-quarter-inch square.

B. Beam Monitor

The beam flux was monitored by a CO_2 - argon-filled ionization chamber. The chamber was filled to a pressure of 64 centimeters of mercury. It had a multiplication factor of 625 for 340 Mev protons, as measured with a faraday cup. The collecting electrode was kept at ground potential by a feedback amplifier located in the counting area. The charge was collected

across a precision condenser located near the electrometer. The voltage across the calibrated condenser was fed to a Speedomax recorder where the charge was automatically recorded continuously. The condenser was discharged when the voltage reached a preset level. N_p, the number of protons monitored by the chamber is given by

$$N_p = \frac{CV}{Me}$$

where C = capacity of precision condenser

V = voltage across the condenser

M = number of ion pairs per proton

e = charge of the electron

As will be seen later, the meson counting equipment was not operating in a "plateau region". Hence it was necessary to normalize the meson detection efficiency from run to run. This normalization compensated for any change in efficiency of the beam monitor from run to run. It was necessary that the monitor remain constant only over the period of a given run.

C. Method of Reducing Beam Energy

When it was desired to reduce the energy of the proton beam, lead absorbers were placed in the beam immediately ahead of the production target. The range-energy curves of Aron, et al.[11], were used to calculate required thicknesses of absorbers. Lead was used for this purpose because it has a high ratio of stopping power to the number of mesons produced[12,13]. These absorbers were placed at the target so that no systematic error in beam monitoring would be introduced by multiple scattering of the proton beam. It was necessary to correct for the beam attenuation in the lead. This correction is discussed later.

If the absorbers had been placed in the collimator ahead of the monitor, the effect of low-energy protons multiply-scattered from the walls of the collimator would have been difficult to estimate. If the absorbers were placed a long distance ahead of the collimator, the above problem would not occur, but the amount of usable beam entering the cave would have given a prohibitively low counting rate.

D. Targets

The polyethylene and carbon targets were shaped in a milling machine so that the area and thickness of each could be measured accurately. The targets were weighed on a chemical balance to about 0.1 gm accuracy, which corresponded to about one part in 2000 for the mass of the targets. The number of grams per square centimeter was calculated from the area and mass. The carbon target was designed to be equivalent to the polyethylene target in grams per square centimeter of carbon.

The targets were held in a movable assembly (shown in Fig. 2), which could be moved from outside the cave. This arrangement eliminated the necessity for turning off the beam to make the frequent target changes necessary in a subtraction experiment.

The target-change assembly, channel, meson absorbers, and crystals were attached to a template which fitted over the poleface, so that the geometry could be reproduced from run to run (see Fig. 2). In order to align the system with respect to the beam, film holders were inserted into positioning holes in the template. Short exposures were taken and the system was aligned with the aid of fiducial marks on the film.

E. Channel

The main function of the channel was to minimize accidental background by preventing high-energy protons from the target from reaching the detector system. The protons whose momenta are small enough to permit them to follow the curve of the channel would not penetrate the copper absorbers, since a proton has a small fraction of the range of a pion for equal momenta. The angle and the energy apertures of the channel were made large compared to the angle subtended by the detector and to the energy interval accepted by the detector. This could be done without relaxing the requirement that high-energy protons from the target should not reach the detector. This design helped to reduce the multiple-scattering correction discussed in Section V.

The angular width of the channel was $\pm$ 7.4°, in comparison with an angular width of $\pm$ 3.0° subtended by the detector. The mean radius of the channel was 16.4 inches. The maximum and minimum radii were 17.4 inches and 15.4 inches, respectively. The energy interval, ΔE, accepted by the channel varied from 13.8 Mev for 70 Mev pions, to 6.9 Mev for 30 Mev pions. In comparison, the ΔE of the detector ranged from 2.6 Mev to 4.1 Mev over the same meson energy interval.

F. Pion Absorbers

The energy of the pions detected was varied by means of copper absorbers. Pion range-energy curves for copper and stilbene were obtained, using the proton range-energy curves of Aron, et al[11]. The magnetic field was changed at each energy setting so that the $H\rho$ for the mean radius of the channel corresponded to a pion whose range was that of the given setting of copper absorbers. Six absorbers were made up in multiples of the smallest, so that

a range of energies from 20 to 80 Mev with approximately 1 Mev intervals was obtainable. The absorbers could be changed from the outside of the cave. This arrangement eliminated the necessity of turning off the cyclotron.

G. Detectors

1P21 photomultipliers viewing trans-stilbene crystals through lucite light pipes were used as pion detectors. Since the phototubes are sensitive to magnetic fields, they were placed outside the magnet coils in a region where the field was approximately 100 gauss. In addition, the phototubes were enclosed in a 1/16-inch mild steel housing, which was in turn enclosed in a 1/4-inch thick steel shield. In order to obtain practical counting rates, it was necessary to detect the pions near the target in a region of high field. Lucite light pipes served to optically connect the phototubes outside the coil case with the crystals near the target. The light pipes and magnetic shields are shown in Fig. 2. Tests were made to check the variation of the phototube sensitivity with the variation of the field in the gap. Using a γ-ray source, a change of one part in sixty in pulse height was observed for a variation of 7000 gauss in the field in the gap. Since the range of field strengths employed in the experiment was 4000 gauss, the effect was negligible.

H. Method of Pion Detection

1. Introduction

The detection method is based on the principle of identifying the positive pions by their characteristic decay to muons.

$$\pi^+ \rightarrow \mu^+ + \nu$$

The mean life of the positive pion has been measured to be 0.0257 microseconds.[14,15] A crystal telescope is exposed to the beam of particles, and the number of delayed coincidences between positive pions and their decay muons are counted as positive pions.

In the early stages of the experiment, a two-crystal telescope was in use with one delayed coincidence circuit[15]. In the earlier scheme, the coincidence caused by a positive pion passing through the first crystal and penetrating the second far enough to lose approximately 6 Mev, generated a gate which was delayed and put in coincidence with another output from the second crystal. If the pion decayed in the second crystal during the time the gate was actuated, a delayed coincidence was registered as a positive pion. In order to measure accidental background, the delay was increased to a time where all positive pions would have previously decayed. The count at that time was recorded as background and subtracted from the count taken at the short delay.

This arrangement was undesirable in that it required running the background separately. For a given integrated proton flux the pion count is constant, but the accidental background varies linearly with the beam intensity. Since the background rate for this equipment operating in the cave was of the same order as the pion rate, any shift in beam intensity between the short and the long delay counts made reproducibility poor. This difficulty is intensified in a subtraction experiment. For this reason, a second delayed coincidence π-μ circuit was constructed so that the accidental background could be counted simultaneously with the pion data. The use of two circuits also doubled the overall efficiency in terms of cyclotron operating time. One detector was run with the short delay while the other

was run with a long delay and then the delays were interchanged for an equivalent integrated beam flux.

Under these conditions, lack of reproducibility due to beam intensity changes enters only as the product of the difference in intensity and the difference in efficiency between the two detectors. The difference in efficiency was made small. The arrangements made to change absorbers and targets without turning off the beam aided the reproducibility since the beam intensity is much more constant when the machine is not turned off frequently.

In the previous set-up, plateaus were not obtained for the pion pulses used in generating gates. As a solution to this problem the two-crystal telescope was replaced by a three-crystal telescope. The first two crystals were used for generating the gate, and only the delayed pulses of the muons were taken from the third crystal. In this way plateaus were obtained for the gate-opening pion pulses. In order to detect low-energy pions, the crystals were made much thinner, resulting in smaller signals. A new distributed coincidence circuit was constructed to operate with these low signals. This equipment was used in the measurements and is described in the following sections.

2. Description of the Method

Figure 3 shows a schematic diagram of the detection system. A positive pion passing through the first two trans-stilbene crystals causes scintillations which are transmitted through light pipes to 1P21 photomultipliers 1 and 2. The signals from these photomultipliers are amplified by distributed amplifiers A and B, and fed to a distributed coincidence. The output of the coincidence circuit is delayed and sent to gate generators 1 and 2.

The variable delay is obtained by using different lengths of RG63/U coaxial cable to transmit the signal. The gate generators are non-symmetrical cathode-coupled multivibrators with a fixed discrimination level. They produce gates approximately 0.07 microsecond in length. The outputs of the gate generators are scaled and sent to the π-μ coincidence circuits.

The output of the third photomultiplier is amplified by distributed amplifiers 1 and 2, and fed to the π-μ coincidence circuits. In normal operation, the delays on the gates referred to above are so adjusted that if a particle appears in the third crystal in the time interval 0.02 to 0.09 microsecond after the coincident pulses in the first two crystals, it will make a delayed coincidence with the gate in one of the π-μ coincidence circuits and will be scaled as a positive pion. If the signal appears in the time interval 0.19 to 0.26 microsecond, it will make a delayed coincidence with the gate in the other π-μ coincidence and will be scaled as background. The delays are then interchanged for an equivalent integrated proton beam flux. The delays are changed from the counting area by coaxial switches operated by 110-volt relays.

3. Description of Electronics

The distributed amplifiers A and B and the distributed coincidence[16] shown in Fig. 3 were built as a unit. The circuit diagram is shown in Fig. 4. The amplifiers deliver a maximum positive signal of about 8 volts into a 190-ohm load with a gain of about forty. The coincidence resolution of the circuit was measured with protons passing through two crystals. The test was made with the crystals on 28-inch light pipes, and no attempt was made to clip the pulses. When a delay of 0.018 microsecond was inserted

in one side, all counts above accidental background disappeared. A resolution of 0.01 microsecond was measured using a pulse generator with a signal output about 0.008 microsecond in length. The ratio of voltage out with a signal in both sides to voltage out with a signal in one side is better than ten to one.

The units labeled gate generator 1 and π-μ-1 coincidence circuit in the schematic Fig. 3 were built into one chassis. A similar chassis contains the units designated by number -2. The circuit diagram for each of these units is shown in Fig. 5.

4. Plateaus, Counting Efficiencies

The plateaus of pion counting rate versus photomultiplier voltage on the first two detectors in the telescope are shown in Fig. 6. These plateaus indicate full efficiency for generating a gate if a positive pion enters the telescope. No satisfactory plateau was obtained for the decay muon pulses from the third crystal. There seemed to be some evidence of a short region where the pion counting rate versus the third photomultiplier voltage had a reasonable slope; but since it was not sufficiently defined to be used for determining operating levels, the following method was employed:

The magnetic field was set so that the mean $H\rho$ of the channel corresponding to positive pions with a kinetic energy of sixty-two Mev. The copper absorbers which would ordinarily degrade these pions to twenty-one Mev so that they would stop in the detector, were then removed. Under these conditions a greatly increased flux of pions and scattered protons were entering the detector. All pions should pass on through the detector and not be counted except for a very few pions which might be scattered

from the channel walls with energies in the proper interval to be counted.

At low voltages (approximately 1200 volts) on photomultiplier three a few mesons compatible with the number which might scatter from the walls were observed. As the voltage was increased this number remained approximately constant until the voltage reached 1400 volts. Above that point a sharp break in meson counting rate appeared. The voltage was then lowered below this point. The absorbers were replaced so that the positive pions would stop in the detector, and a half-life was run on the particles by varying the delay of the gate. When this was done, the half-life measured agreed with the published values[14,15].

A number of reasons may be advanced to explain the lack of a clear-cut plateau on the muon pulses:

1. The 1.2 millimeter range of a 4 Mev muon is comparable with the 8.8 millimeter thickness of the crystal so that there is one muon with a partial path in the detector crystal for every six whose paths lie completely within the crystal. This number includes those which leave the crystal and those which enter from the outside. This effect would contribute a finite slope to any plateau obtained.

2. The use of long light pipes will cause the statistical fractional fluctuations in pulse height to be larger than the relative fluctuations encountered when no light pipes are used[17].

3. The light collection efficiency may vary over different portions of the crystal.

These effects would account for a slope over the region of pion detection. One must finally account for the indefinite increase beyond the possible number of mesons present as the voltage on the photomultiplier is

increased. As the voltage is increased, the pulses due to stopping protons may be very large. This causes the distributed amplifier to saturate and broaden the amplified pulses. This broadening persists into the time interval that the gate is open when a short delay is employed, and makes a delayed coincidence. When the long delay is used, the broadened pulse disappears before the gate rises and no delayed coincidence results.

In order to show that this condition was not present at the operating point chosen and that the detector was not sensitive to secondary "satellite" pulses believed to follow the main pulses[18] in a photomultiplier, a test was made with 32 Mev protons from the Berkeley proton linear accelerator. With 2×10^5 fifteen-Mev protons entering the detector crystal, a total of sixty-one delayed coincidences were made. Of these, twenty-eight occurred at the short delay and thirty-three at the long delay, giving a net difference of five plus or minus eight. Furthermore, it is almost certain that many of these were accidental coincidences as they were correlated with "bursts" of protons from the machine. Under normal conditions of the experiment, between six-hundred and twenty-five hundred pions would have been counted for an equivalent number of particles entering the detector, so the effect is negligible.

Since no plateau was obtained, it was necessary to have a check on the stability of the detection efficiency. The number of positive pions from the carbon target for a certain integrated proton flux and for a particular meson energy was used as a standard point. Carbon was chosen since its spectrum is slowly changing, and the yield at this point would not be sensitive to small changes in the proton beam energy. This point was measured at intervals of five to six hours during all runs. A plot of these points

for two runs is given in Fig. 7.

5. Background

The accidental background rates encountered in the experiment ranged from thirty-five per cent to three hundred per cent of the meson counting rate, depending upon the target and proton energy. The scattered proton beam has a radiofrequency structure such that short bursts of particles occur about 0.06 microsecond apart. This interval is of the same order as the gate length employed in the π-μ coincidence. At the short delay the gate spans only one of these r-f bursts so that it was necessary to insure that the gate spanned only one r-f burst at the long delay. The long delay was varied in steps of about 0.015 microsecond, and a variation of the same periodicity as the r-f frequency of the beam was observed. The long delay was chosen to correspond to a minimum so that the gate overlapped only one r-f burst.

6. Validity of Detection

Evidence for the validity of positive pion detection by this system is presented by the following: The positive pion mean life was observed with the system[15] and a value obtained which is in excellent agreement with that obtained by Wiegand[14]. Experiments were conducted at the Berkeley synchrotron on the photoproduction of pions from hydrogen, deuterium[19], and helium[20]. Pions were detected with nuclear emulsions as well as with this system. When the counter data were normalized to the emulsion data for one gas, the data for the two methods of detection agreed for the other two gases. When the efficiency of the system is obtained by normalizing the hydrogen data to Cartwright's hydrogen data for absolute values, a

differential cross section $d\sigma/d\Omega\, dE = 13.7 \times 10^{-30}$ cm^2 Mev^{-1} sterad^{-1} is obtained for carbon at 70 Mev. This is to be compared with the value $d\sigma/d\Omega\, dE = 12.3 \times 10^{-30}$ cm^2 Mev^{-1} sterad^{-1} obtained by Cartwright[3c]. The agreement is within the statistics of either experiment.

V. ANALYSIS OF THE DATA

A. Corrections

1. Introduction

Four corrections were applied to the data. It was necessary to correct for:

1. The attenuation of the proton beam in the lead absorbers,
2. The decay of the pions in flight,
3. The absorption of the pions in the Cu absorbers, and
4. The loss of pions due to multiple scattering.

Finally, it is shown that no correction need be made for delayed coincidences arising from the beta decay of the positive muons stopped in the region of the detector.

2. Attenuation of the Proton Beam in the Pb Absorber

Attenuation of the proton beam in the lead absorbers occurred in two ways. Elastic collisions which deflect the protons from the beam direction cause the probability of detecting the reaction to decrease for these protons because the cross section for production of a pion is a function of angle. Any inelastic collision suffered by a proton with a lead nucleus removes it from the usable beam, as any pion produced by it would fall out of the narrow energy range scanned in the experiment.

The elastic scattering may be nuclear or multiple-coulomb scattering. The data of Richardson, et al[21], indicates that for the thickest lead absorber used here, only four per cent of the protons would suffer elastic nuclear collisions. Of these, only a few per cent would be scattered as much as five degrees; and, since the production probability is only down

by four per cent at five degrees, the effect is negligible.

Multiple scattering of the protons does give rise to the need for a small correction. Using the formulas

$$P(\theta) = Ne^{-\theta^2/2\overline{\theta^2}}$$

where N = normalizing factor

P(θ) = probability per unit angle of scattering into dθ at the angle θ

θ = angle of the scattered particle

$\overline{\theta^2}$ = mean square scattering angle

$$\overline{\theta^2} = \left[\frac{16\pi A Z^2 e^4}{M v^2 p^2} \ln 183 Z^{-1/3}\right] \xi$$

where A = Avogadro's number

M = molecular weight of absorbing material

Z = atomic number of absorbing material

e = charge of the electron

v = velocity of particle

ξ = thickness of absorber in gms/cm^2

the angular distribution of the scattered protons was obtained for each absorber. These angular distributions were combined with the production probability obtained from the known $\cos^2\theta$ center of mass angular distribution for the reaction $(pp \longrightarrow \pi^+ d)$[3]. The resulting maximum correction was 1.6 per cent for this effect.

The second part of the proton attenuation correction is for inelastic scattering. The inelastic scattering cross section for 340 Mev protons on lead has not been measured. An estimate of this correction was made from

other scattering data. Richardson[21] measured the total inelastic cross section for 340 Mev protons on copper and obtained a cross section of about 0.7 of the total neutron cross section measured by Moyer and DeJuren[22]. Ball[23] obtained a tentative value for inelastic scattering of 340 Mev protons on tungsten equal to about 0.5 of the total neutron cross section.

The correction was made here using σ (inelastic) = 1.75 barns, which is slightly greater than 0.6 of the total 270 Mev neutron cross section[22]. The attenuation is given by the relation

$$N = N_0 e^{-\frac{A}{M}\sigma\xi}$$

where A = Avogadro's number

M = molecular weight of lead

σ = cross section for inelastic scattering of protons in Pb

ξ = thickness of Pb absorber in gms/cm^2.

N is the number of particles available at the production target if N_0 is the number monitored by the ionization chamber. The correction factors for the various absorbers due to inelastic nuclear scattering are given in Table I.

TABLE I.

Proton Attenuation Correction

Proton Energy (Mev)	Correction Factor
336	1.000
330	1.015
325	1.029
321	1.046
315	1.061
311	1.078

3. Pion Decay in Flight

Since the positive pions are detected by their decay into positive muons after stopping in the detector, those which decay in flight between the production target and the detector are lost. The number lost varies with pion energy, as the transit time in the pion frame of reference is a function of the energy of the pion.

For N pions detected, the number N_o leaving the target would be

$$N_o = N e^{t/\tau}$$

where t = transit time in pions frame of reference

τ = mean life of positive pion 2.57×10^{-8} sec.[14,15]

Equating the dilated proper time in the pion frame to the time measured in the laboratory, and using the relativistic expression for velocity in the laboratory frame, one obtains for the transit time in the pion frame between points a and b in the laboratory the expression

$$t = \frac{E_o}{c} \int_a^b \frac{dx}{\sqrt{T(T+2E_o)}}$$

where t = time in pion frame in seconds

E_o = rest energy of positive pions

T = kinetic energy of pions in laboratory system

This expression was integrated numerically over the range of pion energies detected, and a correction was obtained ranging from twelve per cent at the lowest energies detected to seven per cent at the highest.

4. Nuclear Attenuation of Pions in Copper Absorbers

The correction for nuclear attenuation of the pions in the copper absorbers was made using nuclear area given by $\sigma = (1.37A^{1/3})^2 \times 10^{-26}$ cm^2 = 0.94 barns obtained from neutron scattering[24]. This value is in agreement

with the values published for 85 Mev negative pions[25]. Preliminary reports on positive pion absorption in heavy nuclei indicate the values may be a little smaller than those for negative pions and that they increase with increasing energy. This variation with energy would tend to lower the excitation points nearest threshold, but the correction is small and the results would not be changed appreciably.

N_o, the number of pions entering the copper absorber, is given by

$$N_o = N e^{\frac{A}{M}\sigma\xi}$$

where N = number of pions detected

A = Avogadro's number

M = molecular weight of Cu

σ = absorption cross section for pions on Cu

ξ = thickness of Cu absorber gm/cm^2

The correction ranged from two per cent to eighteen per cent for the pion energies detected.

5. Multiple Scattering Loss of Pions in the Copper Absorbers

The pion channel was designed in such a way that its exit was wide compared to the area of the detector telescope to minimize multiple scattering effects; however, crystals 1 and 2 of the coincidence telescope are only slightly larger in area than the muon detector crystal, and hence for the outer edges of the muon detector crystal they define the entrance aperture.

For a thickness t of copper absorber, the projected displacement Y in a plane containing the line of the pion beam and at a distance L beyond the

end of the copper absorber (the distance to the center of the muon detector crystal) has a distribution function given by

$$F(tY) = \frac{\exp - \left[\frac{Y^2}{4(A_0L^2+2A_1L+A_2)} \right]}{2\sqrt{\pi}\sqrt{A_0L^2+2A_1L+A_2}}$$

where A_0, A_1, A_2 are functions of t. The derivation of the distribution function is outlined in the Appendix, and the definitions of the A's are given there. This distribution function is derived taking into account the loss of energy of a particle as it penetrates the material.

At seven points across the muon detector crystal, the distribution function was integrated between the values of the projected displacement Y determined by the entrance aperture as seen from that point of the crystal. This procedure was carried out for a number of absorber thicknesses. The fraction of particles lost at each of the seven points was plotted, and the total loss for the whole crystal calculated from the area of the curve. The correction factor ranged from 1.02 to 1.13 for the pion energies detected.

6. Effect of Muon Decay

Since the detection method requires stopping the pions in a crystal and detecting the 4 Mev muons emitted when the positive pions decay, there will be a large number of $\mu^+ \rightarrow \beta^+$ decays in the vicinity of this crystal. The equation for the activity of a daughter decay product may be set up using the law for radioactive decay and then integrated over the times that the gate is open. Approximately three per cent of all the $\mu^+ \rightarrow \beta^+$ decays occur during either the short or long delay gate, and the difference is less than one tenth of a per cent of all decays. In addition to this limitation based

on time, geometrical considerations would further limit the number of betas which might be counted. Hence the effect of muon decay may be neglected.

B. Fitting Curves to the Data

At each proton energy a set of polyethylene points with a peak structure was obtained (See Figs. 9 to 14). The curves for these peaks were drawn visually. On the low-energy side of the peaks the slope on the upper part of the peak was extrapolated down to the carbon line, since the contribution from the reaction $p + p \longrightarrow \pi^+ + p + n$ might be expected to alter the slope near the low-energy edge of the peak. The 336 Mev proton point was corrected for the contribution expected from this reaction, using the calculated energy resolution of the system and the measured $p + p \longrightarrow \pi^+ + p + n$ yield below the peak. This correction amounted to five per cent of the area at this energy. Insufficient data was taken to calculate the corrections at some of the other proton energies; however, the energy interval between the upper limit of the continuum and the line spectrum increases from 4.2 Mev at the 336 Mev proton point to 5.1 Mev at the lowest proton energy. This increase in the separation would tend to decrease the contribution of pions from the ($pp, \pi^+ pn$) reaction. Furthermore, in the two additional cases (Ep = 326 Mev, 321 Mev, see Figs. 11, 12) where points were obtained below the peak, the yield from the ($pp, \pi^+ pn$) reaction appears to be too small to introduce any appreciable contribution.

The carbon spectrum at each proton energy is relatively flat. Consequently, it was assumed that a straight line could be used to represent the spectrum over the pion energy interval involved, and the method of least squares[26] was used to obtain the constants for the line.

The area between the polyethylene curve and the carbon curve represents the hydrogen contribution. The areas were obtained by counting squares and were checked with a planimeter.

C. Estimation of Errors

The standard deviations for the constants of the straight line representing the carbon spectrum were computed, and the error in the area under the carbon line was obtained with them. For the polyethylene data a second curve was drawn to fit the end points of the standard deviations of the individual points. The area between this curve and the curve best fitting the points was divided by the square root of the number of points used in fitting the data, and the result was taken to be the standard deviation of the polyethylene area. This deviation and the one for the carbon area were then compounded as the square root of the sum of the squares of the individual deviations to yield a standard deviation for the difference area.

Since the detection efficiency was not necessarily constant, it was necessary to normalize from one run to another by means of the standard data point mentioned earlier. This procedure introduced another statistical deviation which depended on the statistical accuracy with which the standard point was counted on a given run. Most of the pion curves for a given proton energy were observed in at least two separate runs, and this tends to decrease the normalization error. The standard deviations due to normalization were computed and compounded with those indicated in the previous paragraph. The resultant standard deviations ranged from 7.5 per cent to 12.5 per cent.

D. Normalization for Absolute Values

Since the efficiency of the detection scheme was not known, it was necessary to obtain an absolute value for the differential cross sections by comparison with values obtained by a method of known efficiency. The 336 Mev proton data obtained here were normalized to the 340 Mev data of Cartwright[3c] measured with nuclear emulsion detectors. His 340 Mev value of $d\sigma/d\Omega$ ($pp \longrightarrow \pi^+ d$ at 0°) = $1.3 \pm 0.3 \times 10^{-28}$ cm^2 $sterad^{-1}$ was extrapolated to $d\sigma/d\Omega = 1.22 \pm 0.3 \times 10^{-28}$ cm^2 $sterad^{-1}$ at 336 Mev, using the relative excitation function measured in this work.

In Section V C, statistical deviations arising in this experiment were discussed. The relative values of the differential cross sections at different proton energies are as good as the statistical errors obtained there; however, the absolute values are only as good as the figure used for normalization, which has a twenty-five per cent deviation.

E. Asymmetry of the Pion Spectra of Polyethylene

Inspection of the polyethylene peaks in Figs. 9 through 14 shows that they were all asymmetric in approximately the same way. A number of effects that might give rise to some asymmetry were considered; but when the calculations were made, the effects were much too small to account for the observed asymmetry. It is of interest to note that the same shape of the peak is evident in the data of Cartwright[3c], measured in a different manner and using the deflected beam.

The possibility that the energy distribution of the proton beam was not symmetric about the average energy was then considered. An experiment conducted by Mather and Segrè[27] on range-energy relations for protons had

shown differences between the experimental and the theoretical ionization curves on the low-energy side, for which the authors were not able to account quantitatively. The tentative assumption was made that the asymmetry found in the present experiment was due to the beam distribution, and the predicted distribution was folded into the theoretical ionization curve. The resultant curve was in qualitative agreement with that obtained experimentally by these authors.

VI. RESULTS

Figure 8 shows the spectrum $d\sigma/d\Omega\,dE$ at zero degrees to the beam for the production of positive pions from hydrogen for a proton energy of 336 Mev. The peak due to the reaction ($pp \longrightarrow \pi^+ d$) is shown in relation to the upper part of the continuous spectrum of the reaction ($pp \longrightarrow \pi^+ pn$). Figures 9 through 14 show the pion energy spectra from polyethylene and carbon at each proton energy. Standard deviations are indicated.

The carbon-polyethylene difference is integrated over pion energy for each of the curves to obtain differential cross sections per unit solid angle (at $0^\circ \pm 3^\circ$ to the beam) at each proton energy. Figure 15 shows the excitation function obtained by plotting $d\sigma/d\Omega$ as a function of proton energy in the laboratory system. The threshold point and the observed points are joined by straight lines.

The representation of the data most easily compared with the theoretical discussion of this work is in terms of quantities measured in the center of mass system of the reaction. The differential cross sections in the laboratory and in the center of mass systems of reference are related by the expression

$$\left[\frac{d\sigma(\theta_{CM})}{d\Omega_{CM}}\right] d\Omega_{CM} = \left[\frac{d\sigma(\theta_{LAB})}{d\Omega_{LAB}}\right] d\Omega_{LAB}$$

The relation between the differential solid angles is given by

$$\frac{d\Omega_{LAB}}{d\Omega_{CM}} = \gamma_c \left[\sin^2\theta + \gamma_c^2 \left(\cos\theta - \frac{\beta_c}{\beta_\pi}\right)^2\right]^{1/2} \left(1 - \frac{\beta_c}{\beta_\pi}\cos\theta\right)$$

where θ = laboratory angle of the pion

$C\beta_c$ = velocity of the center of mass frame in the laboratory system

$\gamma_c = 1/\sqrt{1-\beta_c^2}$

$C\beta_\pi$ = velocity of the pion in the laboratory system

This equation may be derived by transforming the pion four-momentum vector from the center of mass frame to the laboratory frame to get relations between the angles in the two frames and then by differentiating the cosine of the angle in one frame by the cosine of the angle in the other. The function is evaluated at zero degrees in the laboratory system for different pion energies, and is used to convert the laboratory measurements to the center of mass differential cross sections. Table II gives the differential cross sections in both systems with the corresponding proton and pion energies.

TABLE II

Differential Cross Sections
In Laboratory and Center of Mass Systems

Laboratory System		Center of Mass System	
E_{proton} Mev	$\frac{d\sigma}{d\Omega}(0^\circ)$ $10^{-30}cm^2sterad^{-1}$	E_{pion} Mev	$\frac{d\sigma}{d\Omega}(0^\circ)$ $10^{-30}cm^2sterad^{-1}$
336	121 ± 9	19.5	31.3 ± 2.3
330	103 ± 8	17.1	25.8 ± 2.0
325	90 ± 10	14.6	21.6 ± 2.4
321	83 ± 10	12.9	18.7 ± 2.0
315	68 ± 8	10.4	14.2 ± 1.7
311	54 ± 7	8.6	10.3 ± 1.3

The center of mass differential cross sections are plotted in Fig. 16 as a function of pion energy. The theoretical curves plotted on the graph are discussed in the following section. Fig. 17 shows the same points plotted with the data of Durbin, Loar, and Steinberger[9]. These authors measured the differential cross section for the reaction ($\pi^+ d \longrightarrow pp$). A differential cross section for the experiment ($pp \longrightarrow \pi^+ d$) is obtained from this inverse cross section by means of the relation[7]

$$\frac{d\sigma}{d\Omega}(pp \rightarrow \pi^+ d) = \frac{3}{4}\frac{q^2}{k^2}\frac{d\sigma}{d\Omega}(\pi^+ d \rightarrow pp)$$

from the theory of detailed balancing. q and k are the pion and proton center of mass momentum respectively.

VII. THEORETICAL DISCUSSION

A discussion of the process $p + p \longrightarrow \pi^+ + d$ has been given by Chew, Goldberger, Steinberger, and Yang[10]. A general interaction is set up containing two terms: $\left[a(q)\ \vec{\sigma}\cdot\vec{\nabla}n\right]$ which leads to pions in even angular momentum states; and $\left[b(q)\ \vec{\sigma}\cdot\vec{q}\right]$ which leads to pions in odd angular momentum states. a(q) and b(q) are scalar functions of the pion center of mass momentum $\vec{q}$. $\vec{\sigma}$ is the nucleon spin operator, and ∇n is a gradient operating on nucleon coordinates only. For the low pion energies considered here it will be assumed that the pions are restricted to s and p states. Other experiments* indicate that the emission is predominantly p state.

On this basis the relation between the measured excitation function and the p wave term, $\left[b(q)\ \vec{\sigma}\cdot\vec{q}\right]$, is considered. If b is assumed to be a constant, this term reduces to one of the terms of a first-order perturbation calculation using pseudoscalar meson theory with pseudovector coupling. In this case the contribution of this term to the cross section has the energy dependence $q^2/k^m E_\pi$, where E_π is the pion total energy in the center of mass frame, k is the relative momentum of the diproton system, and m is at least four and is more probably as large as eight**. The value

---

* 1. For p state emission the reaction $(pp \longrightarrow \pi^0 pp)$ is forbidden. The small cross section observed[28] for this reaction compared to that of the $(pp \longrightarrow \pi^+ d)$ reaction is compatible with a dominant p wave term[29].

2. The constant angular distribution[9] of the reaction $(pp \longrightarrow \pi^+ d)$ with increasing pion energy indicates that only one term is important, as the two terms should have different energy dependences.

3. If the pions are restricted to s and p states, the predominantly $\cos^2\theta$ angular distribution[3b] must come from the p wave.

** The phenomenological theory of Watson, Brueckner[29] makes no prediction for the variation of the possible terms with respect to nucleon momentum. As a result, the theory cannot be applied to the data in such a way as to lead to definite conclusions.

of m depends on the details of the nuclear forces. The cross section is proportional to the product of this factor and a kinematical factor q^E / v_{rel} resulting from the definition of the cross section***, where v_{rel} is the relative velocity of the incoming protons. The energy dependence of the cross section should therefore vary between $q^3 / v_{rel} k^4$ and $q^3 / v_{rel} k^8$. These functions are plotted with the data in Fig. 16. Both curves are normalized to pass through the lowest point, and the data are seen to lie between the two curves.

In this approximation the excitation data of this experiment are consistent with the p wave term, $(\vec{\sigma} \cdot \vec{q})$, in a perturbation calculation using pseudoscalar meson theory with pseudovector coupling. It should be stated that the s wave term, $(\vec{\sigma} \cdot \vec{\nabla}_n)$, does not vanish, but that its coefficient is such that it should be of importance only for pion energies below ten Mev.

The data for higher pion energies obtained by Durbin, Loar, and Steinberger[9], require that the meson nucleon interaction have a higher dependence on the pion momentum than that predicted by this theory, i.e., that the parameter b(q) is an increasing scalar function of q[10].

*** $\frac{d\sigma}{d\Omega} \propto \frac{1}{v_{rel}} |H|^2 \frac{dn}{dE}$ $\qquad \frac{dn}{dE} \propto q E_\pi$

VIII. APPENDIX

The Distribution Function for Multiple Scattering

The expression for the mean square scattered angle of a particle after penetrating a material of atomic number Z for a distance of D centimeters is given by[30]

$$\overline{\Theta^2} = \frac{16\pi N D Z^2 e^4}{v^2 p^2} \ln 183 Z^{-1/3}$$

where v = velocity of the particle

p = momentum of the particle

N = atoms per cm^3

D = distance in the absorber in cm

If the units of length are converted from centimeters to radiation lengths X_o defined by

$$\frac{1}{X_o} = \frac{4\alpha A Z^2 r_e^2}{M} \ln 183 Z^{-1/3}$$

where α = fine structure constant

A = Avogadro's number

Z = atomic number of absorber

M = molecular weight of absorber

r_e = classical radius of the electron

the expression for $\overline{\Theta^2}$ becomes

$$\overline{\Theta^2} = \frac{E_s}{v^2 p^2} t$$

where t = depth in the absorber in radiation lengths

$E_s = \sqrt{\frac{4\pi}{\alpha}}\, mc^2$

m = mass of the electron

C = velocity of light

Rossi and Greisen[30] define a projected scattering angle θ in terms of this scattering angle and set up a diffusion equation for a distribution function F(tyθ) as a function of the distance into the absorber t, the projected displacement y, and the projected scattering angle θ.

$$\frac{\partial F(t,y,\theta)}{\partial t} = -\theta \frac{\partial F(t,y,\theta)}{\partial y} + \frac{1}{\omega^2} \frac{\partial^2 F(t,y,\theta)}{\partial \theta^2} \qquad \omega = 2 \frac{pv}{E_s}$$

If a Fourier transform in y and θ is applied to this equation[31], a change of variables then leads to a separable differential equation for the Fourier transform of F(tyθ) which may be integrated. The solution for the distribution function is obtained from the inverse transform

$$F(t,y,\theta) = \frac{\exp -\left[\frac{A_0 y^2 - 2A_1 y\theta + A_2 \theta^2}{4(A_0 A_2 - A_1^2)}\right]}{4\pi\sqrt{A_0 A_2 - A_1^2}}$$

where

$$A_0 = \int_0^t \frac{dn}{\omega^2(n)} \qquad A_1 = \int_0^t \frac{(t-n)\,dn}{\omega^2(n)} \qquad A_2 = \int_0^t \frac{(t-n)^2\,dn}{\omega^2(n)}$$

For an absorber of thickness t this gives the distribution at the end of the absorber. If the detector is a distance L beyond the end of the absorber, one wishes to obtain the distribution at that point. If the projected displacement at the detector is denoted by Y, then for a given y and θ at the absorber, $Y = y + L\theta$. The distribution of projected displacements at the detector is obtained by making the change of variable $y = Y - L\theta$ in the distribution function above and integrating over θ.

$$F(t,Y) = \frac{\exp -\left[\frac{Y^2}{4(A_0 L^2 + 2A_1 L + A_2)}\right]}{2\sqrt{\pi}\sqrt{A_0 L^2 + 2A_1 L + A_2}}$$

The correction was made with this function as indicated in Section V.

IX. ACKNOWLEDGMENTS

I wish to thank Professor C. Richman for his guidance and support in this problem. I am grateful to Professor B. J. Moyer for help and counsel throughout my graduate research work. I am indebted to Mr. D. Hamlin, Mr. J. Merritt, and Dr. M. J. Jakobson for their assistance throughout the experiment.

Thanks are due Dr. R. S. White for helpful discussions concerning the work. I am grateful to Dr. M. Ruderman for many discussions of the theoretical aspects of the work.

I would like to express my appreciation to the cyclotron operating staff under Mr. J. Vale for their cooperation in making the bombardments.

X. REFERENCES

1. W. F. Cartwright, C. Richman, M. N. Whitehead and H. A. Wilcox, "The Production of $\pi^{\pm}$ Mesons by Protons on Protons in the Direction of the Beam", Phys Rev 78, 823 (1950) and Phys Rev 81, 652(A) (1951)

2. F. S. Crawford, Jr., K. M. Crowe, and M. L. Stevenson, "Evidence Concerning the Reaction $p + p \longrightarrow \pi^{+} + d$", Phys Rev 82, 97 (1951)

3a. W. F. Cartwright, " π^{+}-Meson Mass Determination", Phys Rev 82, 460 (1951).

3b. M. N. Whitehead and C. Richman, "On the Angular Distribution of the $\pi^{\pm}$ Mesons from 341 Mev Protons on Protons", Phys Rev 83, 855 (1951)

3c. W. F. Cartwright, "Production of π^{+}-Mesons by 340 Mev Protons on Protons at 0° to the Beam", Ph.D. Thesis, University of California (1951) UCRL-1278

3d. M. N. Whitehead, "The Angular Distribution of Positive Pions Produced by 340 Mev Protons on Protons", Ph.D. Thesis, University of California (1952)

4. V. Z. Peterson, "Mesons Produced in Proton-Proton Collisions", Phys Rev 79, 407 (1950)
V. Peterson, E. Iloff, and D. Sherman, "Energy Spectrum at 18° of $\pi^{\pm}$ Mesons Produced in Proton-Proton Collisions", Phys Rev 81, 647(A) (1951)

V. Peterson, E. Iloff, and D. Sherman, "Further Evidence Concerning the Reaction $p + p \longrightarrow d + \pi^{+}$", Phys Rev 84, 372 (1951)

5. R. E. Marshak, Rochester High Energy Conference, December, 1950

6. W. Cheston, "On the Reactions $\pi + d \longleftrightarrow p + p$", Phys Rev 83, 1118 (1951)

7. R. Durbin, H. Loar, J. Steinberger, "The Spin of the Pion via the Reaction $\pi^{+} + d \longrightarrow p + p$" Phys Rev 83, 646 (1951)

8. D. L. Clark, A. Roberts, and R. Wilson, "Cross Section for the Reaction $\pi^{+} + d \longrightarrow p + p$, and the Spin of the π^{+}-Meson", Phys Rev 83, 649 (1951)

9. R. Durbin, H. Loar, J. Steinberger, "Absorption of Pions by Deuterons", Phys Rev 84, 581 (1951)

10. G. F. Chew, M. L. Goldberger, J. M. Steinberger, C. N. Yang, "A Theoretical Analysis of the Process $\pi^{+} + d \longleftrightarrow p + p$", Phys Rev 84, 581 (1951)

11. W. A. Aron, B. G. Hoffman, F. C. Williams, "Range-Energy Curves", (Second Revision 1949) AECU-663

W. A. Aron, "The Passage of Charged Particles Through Matter", Ph.D. Thesis, University of California (1951) UCRL-1375

12. D. Clark, "Relative Yield of 20 Mev π^+-Mesons from Seven Elements", Phys Rev 81, 313(A) (1951)

13. D. Hamlin, M. Jakobson, J. Merritt, A. Schulz, " π^+-Meson Production Cross Section as a Function of Atomic Number", Phys Rev 84, 857 (1951)

14. C. Wiegand, "Measurement of the Positive π^+-Meson Lifetime", Phys Rev 83, 1085 (1951)

15. M. Jakobson, A. Schulz, J. Steinberger, "Detection of Positive π-Mesons by π^+ Decay", Phys Rev 81, 894 (1951)

16. C. Wiegand, "Distributed Coincidence Circuit", Rev. Sci. Inst. 21 (12) 975 (1950)

17. R. F. Post, "Resolving Time of the Scintillation Counter", UCRL-1675

See also, Nucleonics, June 1951

18. T. N. K. Godfrey, F. B. Harrison, J. W. Keuffel, "Satellite Pulses from Photomultipliers", Phys Rev 84, 1248 (1951)

19. R. S. White, M. J. Jakobson, A. G. Schulz, "Photomesons from Deuterium", Phys Rev 85, 770(A) (1952)

20. M. J. Jakobson, A. G. Schulz, R. S. White, "The Production of Photomesons from Helium", Phys Rev 85, 772(A) (1952)

21. R. E. Richardson, "Elastic Scattering of 340 Mev Protons", Ph.D. Thesis, University of California (1951), UCRL-1408

22. J. DeJuren, B. J. Moyer, "Variation with Energy of Nuclear Collision Cross Sections for High Energy Neutrons", Phys Rev 81, 919 (1951)

J. DeJuren, "Nuclear Cross Sections for 270 Mev Neutrons", Phys Rev 80, 27 (1950)

23. W. Ball, private communication

24. S. Fernbach, R. Serber, T. B. Taylor, "The Scattering of High Energy Neutrons by Nuclei", Phys Rev 75, 1352 (1949)

25. C. Chedester, P. Isaacs, A. Sachs, J. Steinberger, "Total Cross Sections of π-Mesons on Protons and Several Other Nuclei", Phys Rev 82, 958 (1951)

26. A. G. Worthing, J. Geffner, "Treatment of Experimental Data", New York, J. Wiley and Sons, Inc., 1943

27. R. E. Mather and E. Segrè, "Range Energy Relation for 340 Mev Protons", Phys Rev 84, 191 (1951)

28. B. J. Moyer, R. Madey, R. Hildebrand, N. F. Knable, and R. Hales, "Studies on the Production of Neutral Mesons by Protons", Phys Rev 83, 206 (1951)

29. K. M. Watson and Keith A. Brueckner, "The Analysis of π-Meson Production in Nucleon-Nucleon Collisions", Phys Rev 83, 1 (1951)

30. Bruno Rossi and Kenneth Greisen, "Cosmic Ray Theory", Rev. Mod. Phys. 13, 240 (1941)

31. L. L. Eyges, "Multiple Scattering with Energy Loss", Phys Rev 74, 1535 (1948)

XI. ILLUSTRATIONS

Fig. 1 Schematic diagram of cyclotron and cave showing the trajectory of the external beam. The lower figure gives a detailed layout of the experimental arrangement in the cave.

Fig. 2 Photograph of the channel system. The target change assembly and particle detectors are included.

Fig. 3 Block diagram of the electronics of the detection system.

Fig. 4 Circuit diagram of the distributed coincidence circuit.

Fig. 5 Circuit diagram of the π-μ coincidence circuit.

Fig. 6 Counting rates for pions versus voltage on photomultipliers 1 and 2, respectively.

Fig. 7 Standard data points obtained in two cyclotron runs. The points are for the measured 62 Mev positive pion yield from the carbon target for a fixed integrated proton flux. Standard deviations are indicated.

Fig. 8 The spectrum $d\sigma/d\Omega\, dE$ of positive pions from hydrogen bombarded by 336 Mev protons. The measurements were made at $0^\circ \pm 3^\circ$ to the proton beam direction. Standard deviations are indicated.

Fig. 9 The differential cross sections $d\sigma/d\Omega\, dE\ (0^\circ)$ for positive pions from polyethylene and carbon bombarded by 336 Mev protons. The spectra are shown in the energy region of the peak due to the reaction $p + p \longrightarrow \pi^+ + d$. The curves from which the differential cross section $d\sigma/d\Omega\ (0^\circ)$ for positive pions from hydrogen was obtained are shown. Standard deviations are indicated.

Fig. 10 The differential cross sections $d\sigma/d\Omega\, dE\ (0^\circ)$ for positive pions from polyethylene and carbon bombarded by 331 Mev protons. The spectra are shown in the energy region of the peak due to the reaction $p + p \longrightarrow \pi^+ + d$. The curves from which the differential cross section $d\sigma/d\Omega\ (0^\circ)$ for positive pions from hydrogen was obtained are shown. Standard deviations are indicated.

Fig. 11 The differential cross sections $d\sigma/d\Omega\, dE\ (0^\circ)$ for positive pions from polyethylene and carbon bombarded by 326 Mev protons. The spectra are shown in the energy region of the peak due to the reaction $p + p \longrightarrow \pi^+ + d$. The curves from which the differential cross section $d\sigma/d\Omega(0^\circ)$ for positive pions from hydrogen was obtained are shown. Standard deviations are indicated.

Fig. 12 The differential cross sections $d\sigma/d\Omega\, dE\ (0^\circ)$ for positive pions from polyethylene and carbon bombarded by 321 Mev protons. The spectra are shown in the energy region of the peak due to the reaction $p + p \longrightarrow \pi^+ + d$. The curves from which the differential cross section $d\sigma/d\Omega\ (0^\circ)$ for positive pions from hydrogen was obtained are shown. Standard deviations are indicated.

Fig. 13 The differential cross sections $d\sigma/d\Omega\, dE\ (0^\circ)$ for positive pions from polyethylene and carbon bombarded by 316 Mev protons. The spectra are shown in the energy region of the peak due to the reaction $p + p \longrightarrow \pi^+ + d$. The curves from which the differential cross section $d\sigma/d\Omega\ (0^\circ)$ for positive pions from hydrogen was obtained are shown. Standard deviations are indicated.

Fig. 14 The differential cross sections $d\sigma/d\Omega\, dE\ (0^\circ)$ for positive pions from polyethylene and carbon bombarded by 311 Mev protons. The spectra are shown in the energy region of the peak due to the reaction $p + p \longrightarrow \pi^+ + d$. The curves from which the differential cross section $d\sigma/d\Omega\ (0^\circ)$ for positive pions from hydrogen was obtained are shown. Standard deviations are indicated.

Fig. 15 The cross section (in the laboratory system of reference) $d\sigma/d\Omega\,(0^\circ \pm 3^\circ)$ for the reaction $p + p \longrightarrow \pi^+ + d$ plotted as a function of proton kinetic energy in the laboratory system. The threshold point at 291 Mev and the observed values are connected by straight lines. Standard deviations are indicated.

Fig. 16 The cross section (in the center of mass system of reference) $d\sigma/d\Omega\,(0^\circ)$ for the reaction $p + p \longrightarrow \pi^+ + d$ plotted as a function of pion kinetic energy in the center of mass system. The theoretical curves $d\sigma/d\Omega \propto q^3/v_r k^4$ and $d\sigma/d\Omega \propto q^3/v_r k^8$ are plotted. These curves were normalized to fit the point for $E_{\pi\,CM} = 8.5$ Mev. Standard deviations are indicated.

Fig. 17 The center of mass cross section $d\sigma/d\Omega\,(0^\circ)$ for the reaction $p + p \longrightarrow \pi^+ + d$ plotted as a function of pion kinetic energy in the center of mass system. The data for this reaction obtained from the inverse experiment of Durbin, Loar, and Steinberger[9] by detailed balancing are shown.

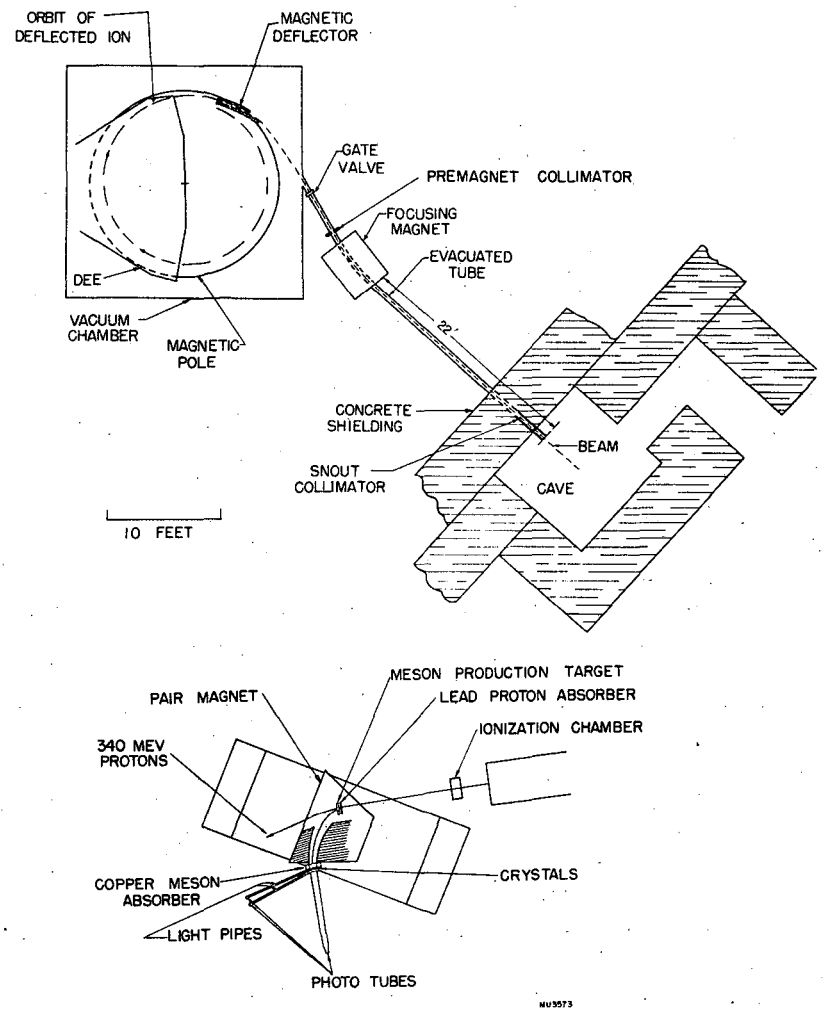
ORBIT OF DEFLECTED ION
MAGNETIC DEFLECTOR
GATE VALVE
PREMAGNET COLLIMATOR
FOCUSING MAGNET
EVACUATED TUBE
DEE
VACUUM CHAMBER
MAGNETIC POLE
22'
CONCRETE SHIELDING
BEAM
SNOUT COLLIMATOR
CAVE
10 FEET
MESON PRODUCTION TARGET
PAIR MAGNET
LEAD PROTON ABSORBER
IONIZATION CHAMBER
340 MEV PROTONS
CRYSTALS
COPPER MESON ABSORBER
LIGHT PIPES
PHOTO TUBES
MU3573

Fig. 1

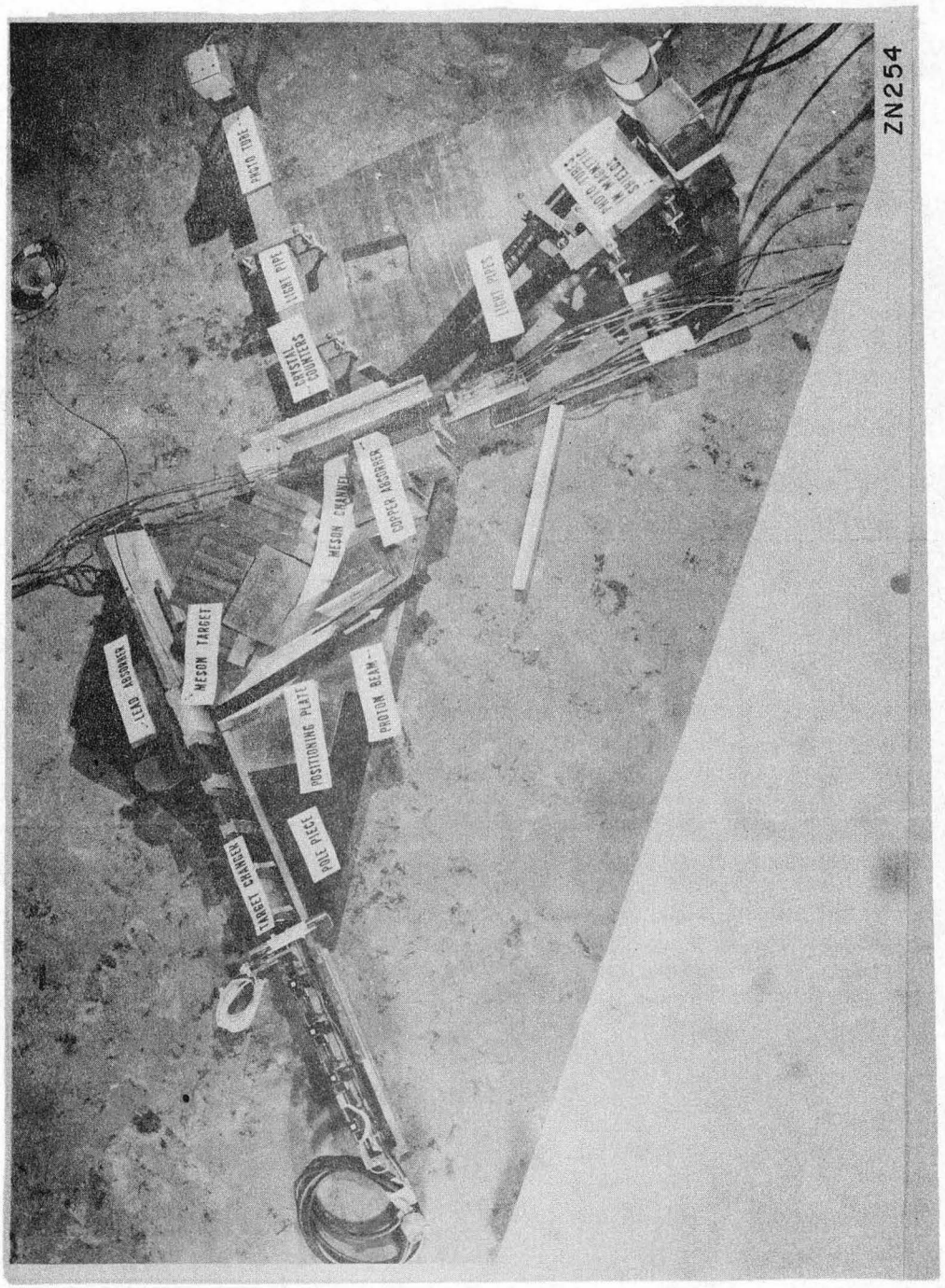
ZN254
LEAD ABSORBER
MESON TARGET
TARGET CHANGER
POLE PIECE
POSITIONING PLATE
PROTON BEAM
MESON CHANNEL
COPPER ABSORBER
CRYSTAL COUNTERS
LIGHT PIPE
LIGHT PIPES

Fig. 2

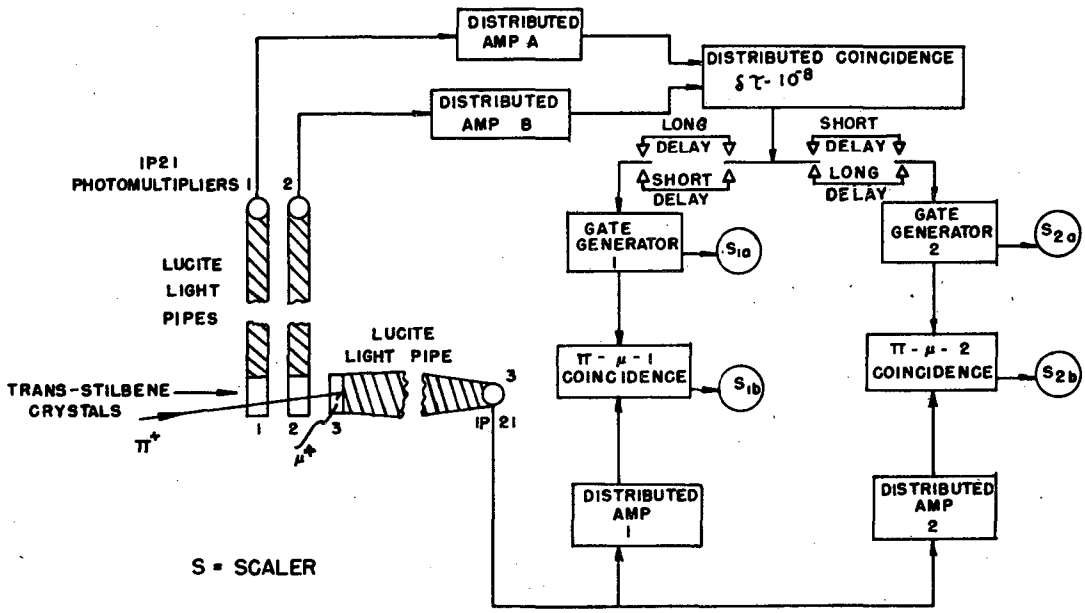

BLOCK DIAGRAM ELECTRONICS

MU3574

Fig. 3

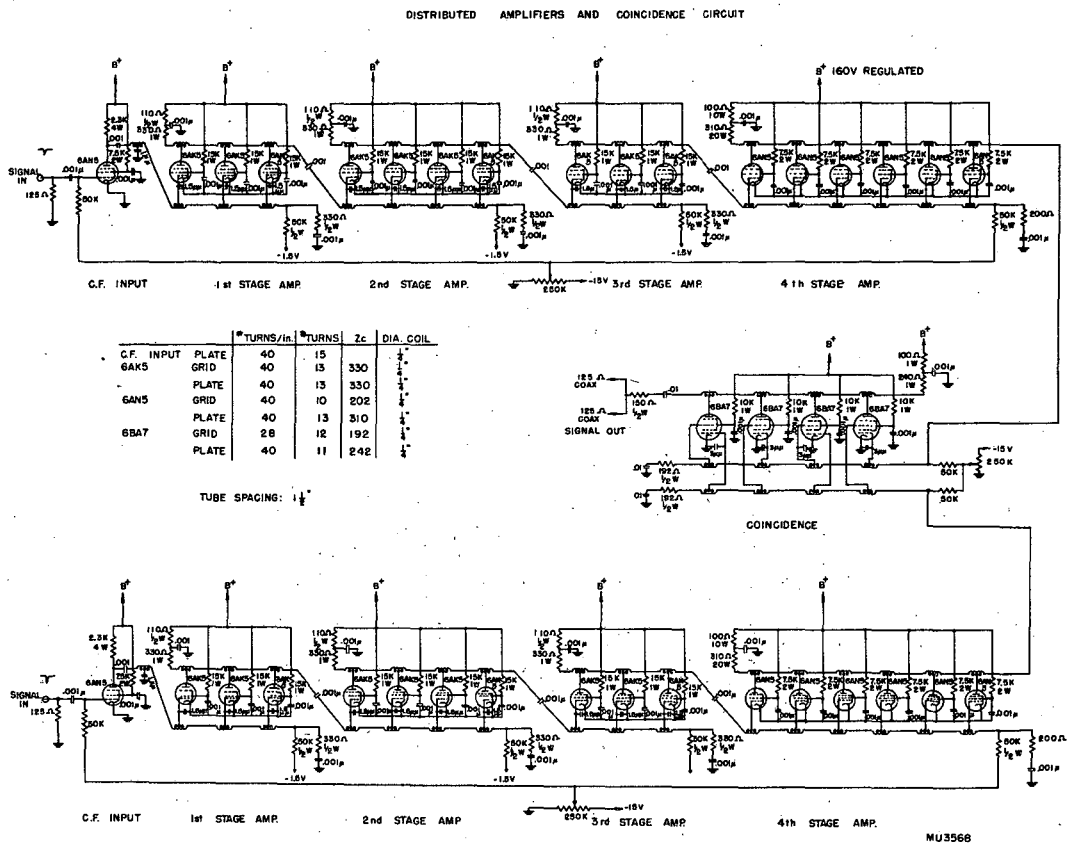

		*TURNS/in.	*TURNS	Zc	DIA. COIL
C.F. INPUT	PLATE	40	15	330	
6AK5	GRID	40	13	330	
	PLATE	40	13	330	
6AN5	GRID	40	10	202	
	PLATE	40	13	310	
6BA7	GRID	28	12	192	
	PLATE	40	11	242	

Fig. 4

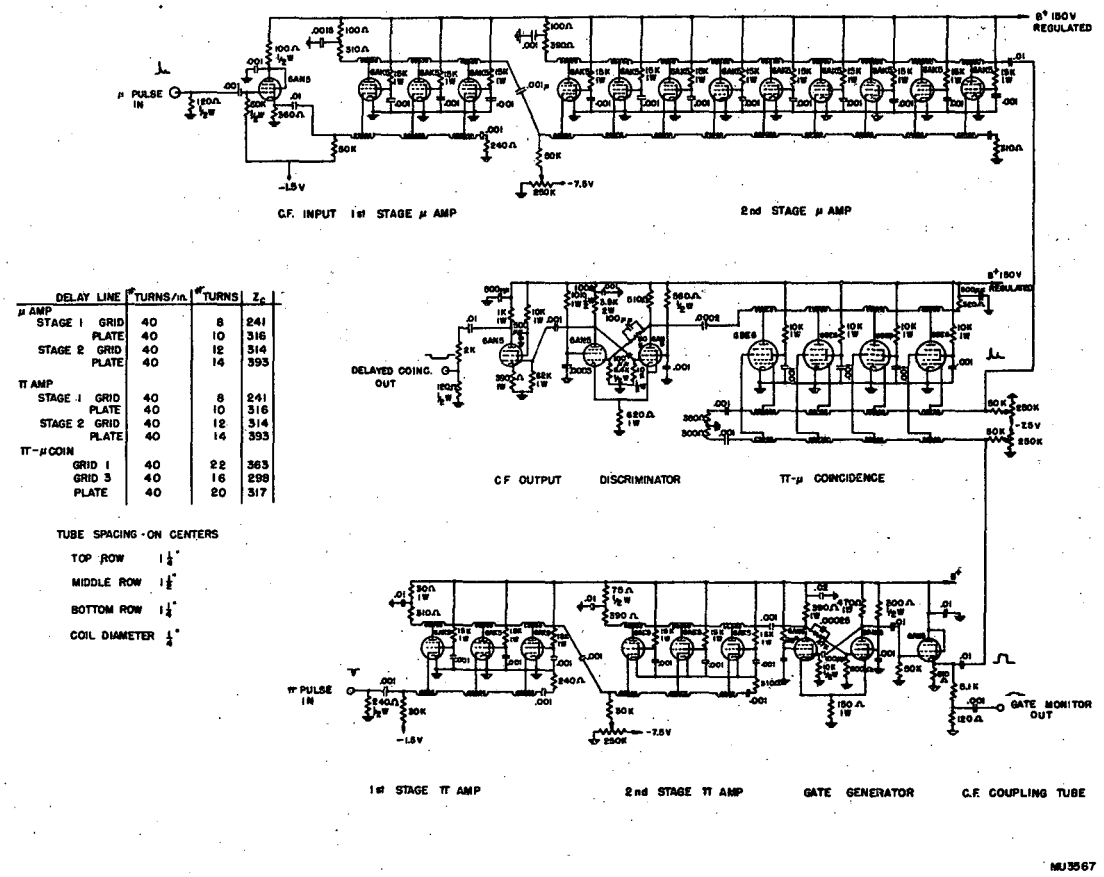

DELAY LINE	TURNS/in.	TURNS	Z_0
μ AMP			
STAGE 1 GRID	40	8	241
PLATE	40	10	316
STAGE 2 GRID	40	12	314
PLATE	40	14	393
TT AMP			
STAGE 1 GRID	40	8	241
PLATE	40	10	316
STAGE 2 GRID	40	12	314
PLATE	40	14	393
TT-μ COIN			
GRID 1	40	22	363
GRID 3	40	16	298
PLATE	40	20	317

TUBE SPACING - ON CENTERS

TOP ROW $1\frac{1}{2}$"

MIDDLE ROW $1\frac{1}{2}$"

BOTTOM ROW $1\frac{1}{2}$"

COIL DIAMETER $\frac{1}{4}$"

Fig. 5

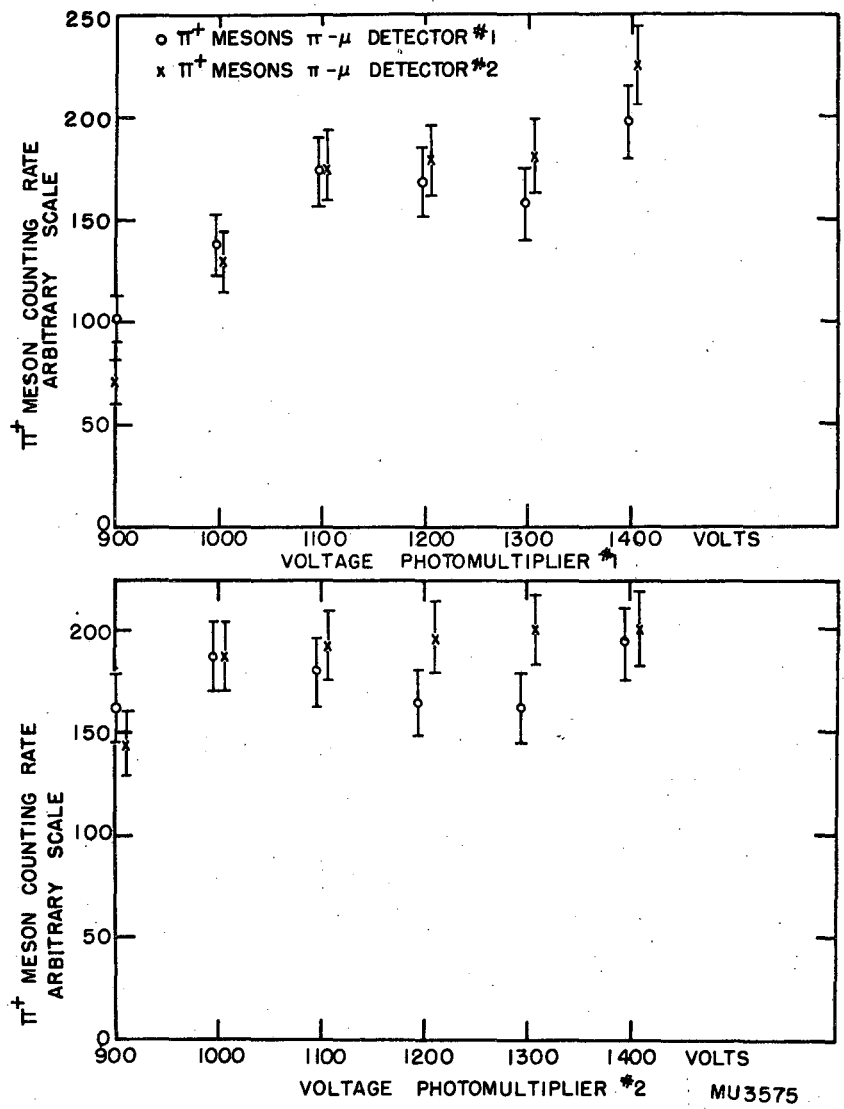
o π+ MESONS π -μ DETECTOR #1
x π+ MESONS π -μ DETECTOR #2
π+ MESON COUNTING RATE ARBITRARY SCALE
250
200
150
100
50
0
900
1000
1100
1200
1300
1400
VOLTS
VOLTAGE PHOTOMULTIPLIER #1
π+ MESON COUNTING RATE ARBITRARY SCALE
200
150
100
50
0
900
1000
1100
1200
1300
1400
VOLTS
VOLTAGE PHOTOMULTIPLIER #2
MU3575

Fig. 6

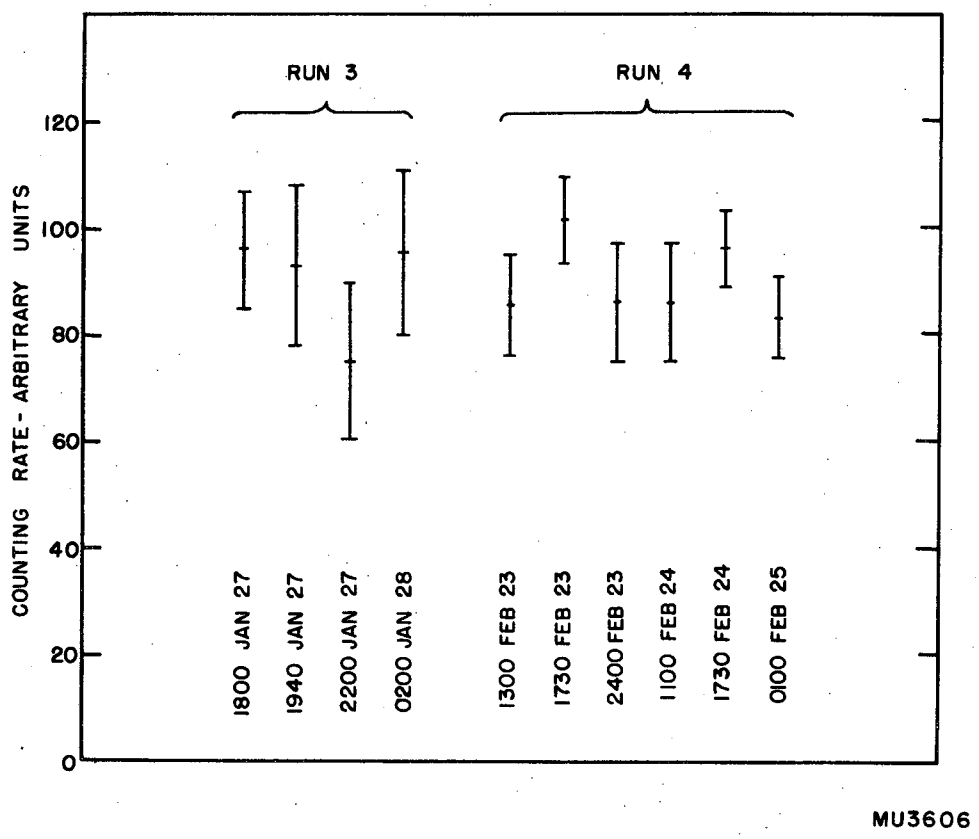
RUN 3
RUN 4
COUNTING RATE - ARBITRARY UNITS
0
20
40
60
80
100
120
1800 JAN 27
1940 JAN 27
2200 JAN 27
0200 JAN 28
1300 FEB 23
1730 FEB 23
2400 FEB 23
1100 FEB 24
1730 FEB 24
0100 FEB 25
MU3606

Fig. 7

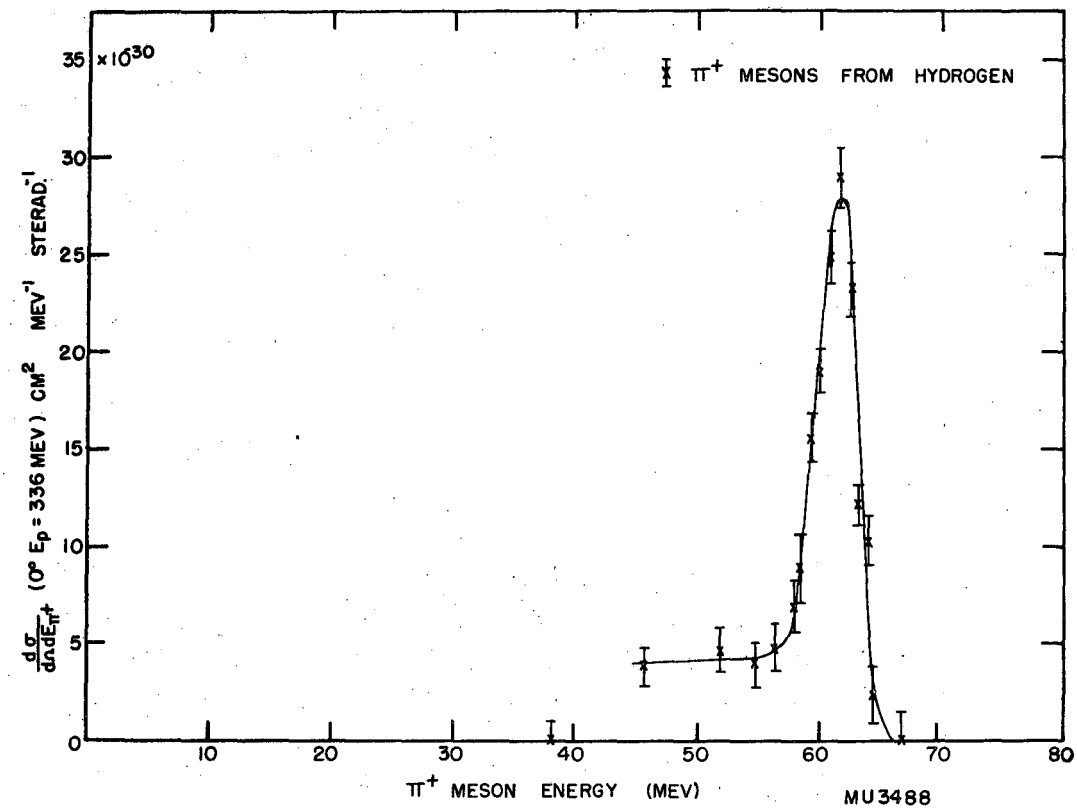
35 x10^30
30
25
20
15
10
5
0
10
20
30
40
50
60
70
80
π+ MESONS FROM HYDROGEN
dσ/dΩdE_π+ (0° E_p = 336 MEV) CM² MEV⁻¹ STERAD.⁻¹
π+ MESON ENERGY (MEV)
MU3488

Fig. 8

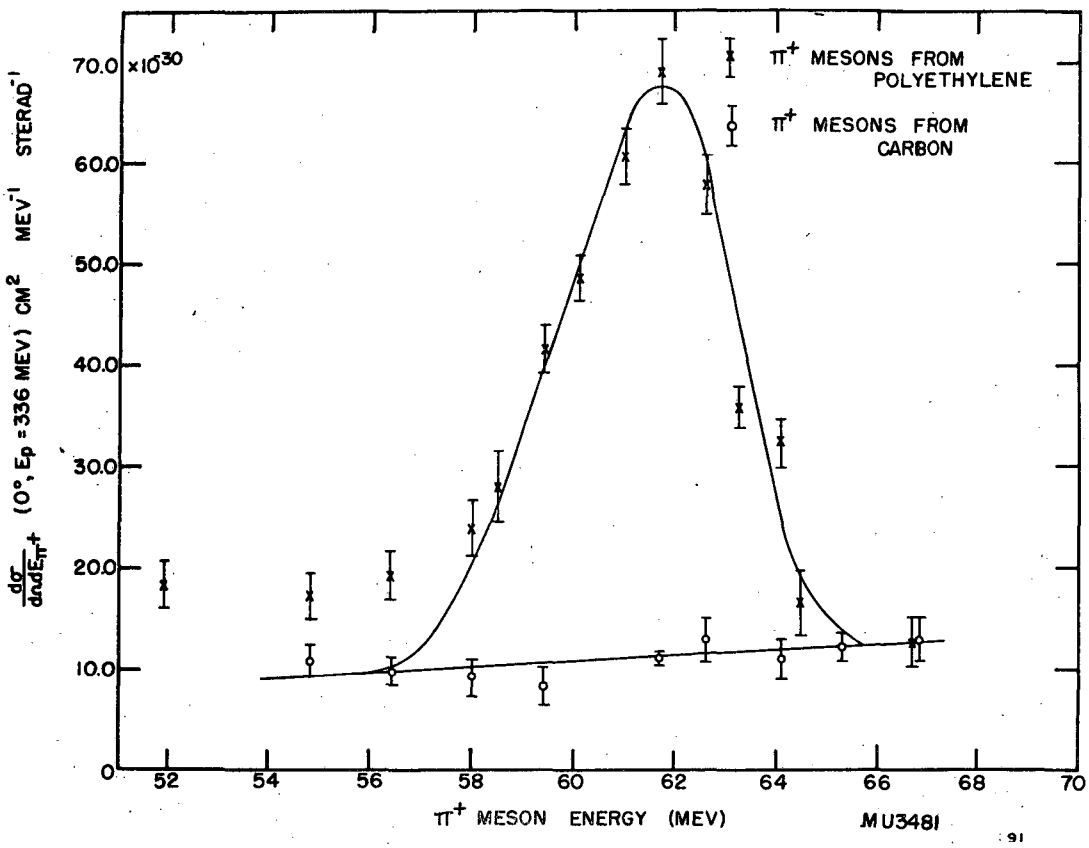
70.0 ×10^30
60.0
50.0
40.0
30.0
20.0
10.0
0
52
54
56
58
60
62
64
66
68
70
π+ MESONS FROM POLYETHYLENE
π+ MESONS FROM CARBON
dσ/dΩdE_π+ (0°, Ep = 336 MEV) CM² MEV⁻¹ STERAD⁻¹
π+ MESON ENERGY (MEV)
MU3481

Fig. 9

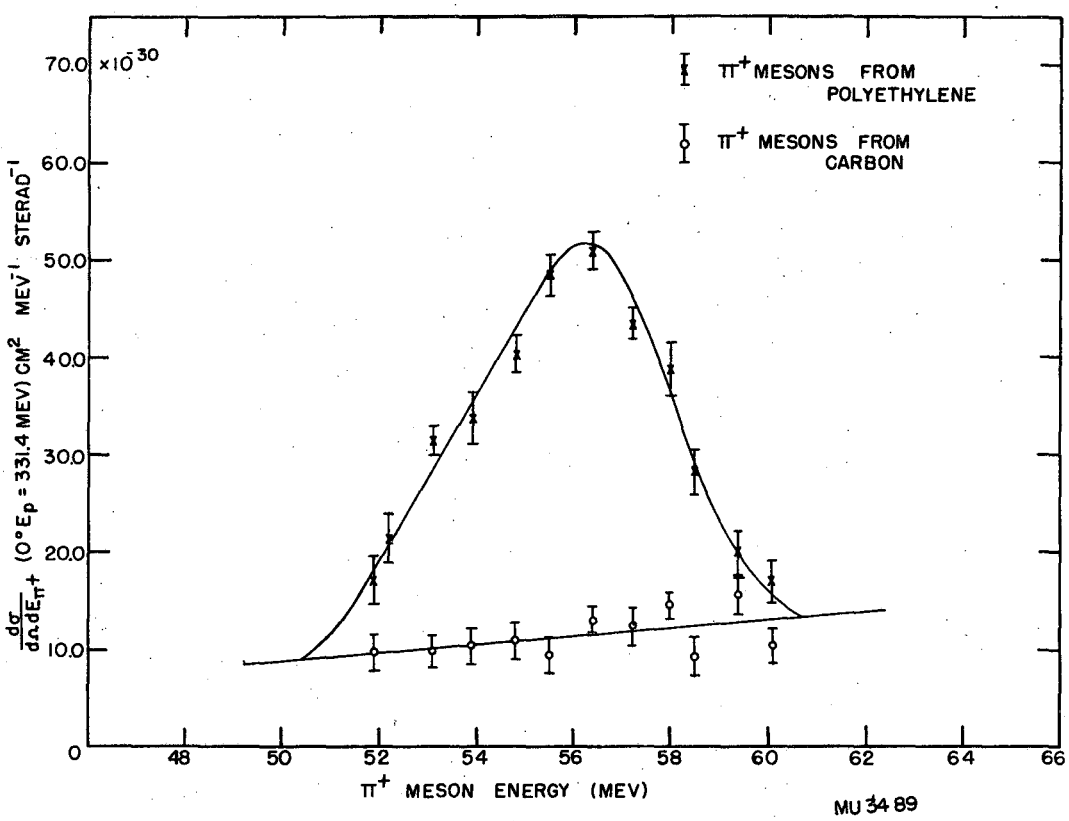
70.0 ×10⁻³⁰
60.0
50.0
40.0
30.0
20.0
10.0
0
48
50
52
54
56
58
60
62
64
66
π⁺ MESONS FROM POLYETHYLENE
π⁺ MESONS FROM CARBON
dσ/dΩdE_π+ (0° E_p = 331.4 MEV) CM² MEV⁻¹ STERAD⁻¹
π⁺ MESON ENERGY (MEV)
MU 34 89

Fig. 10

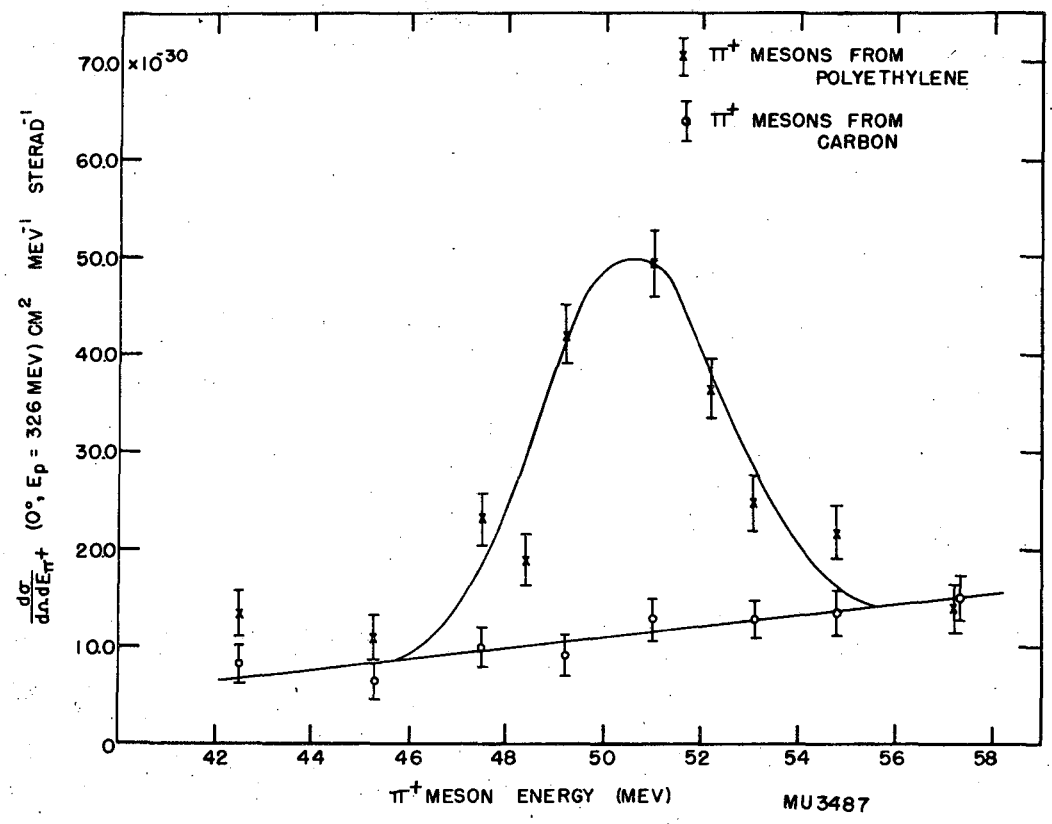
70.0 ×10⁻³⁰
60.0
50.0
40.0
30.0
20.0
10.0
0
42
44
46
48
50
52
54
56
58
π⁺ MESONS FROM POLYETHYLENE
π⁺ MESONS FROM CARBON
dσ/dΩdE_π+ (0°, E_p = 326 MEV) CM² MEV⁻¹ STERAD⁻¹
π⁺ MESON ENERGY (MEV)
MU3487

Fig. 11

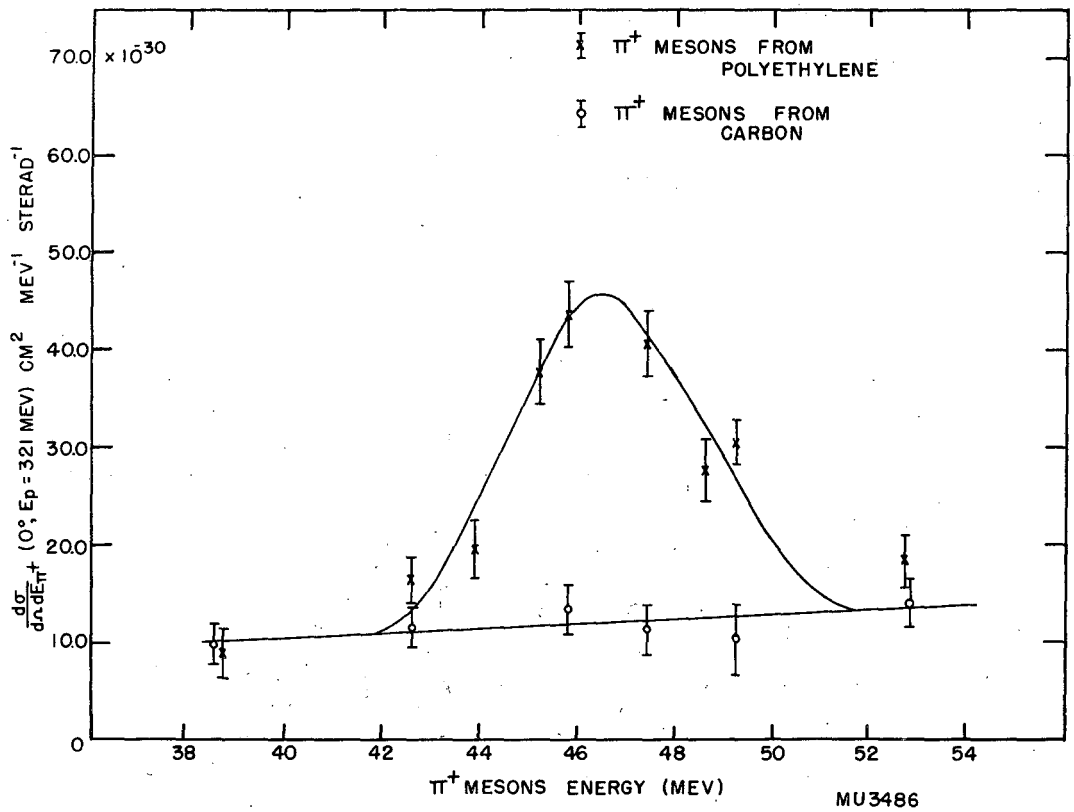
70.0 x 10^30
60.0
50.0
40.0
30.0
20.0
10.0
0
π+ MESONS FROM POLYETHYLENE
π+ MESONS FROM CARBON
dσ/dΩdE_π+ (0°, Ep = 321 MEV) CM^2 MEV^-1 STERAD^-1
38
40
42
44
46
48
50
52
54
π+ MESONS ENERGY (MEV)
MU3486

Fig. 12

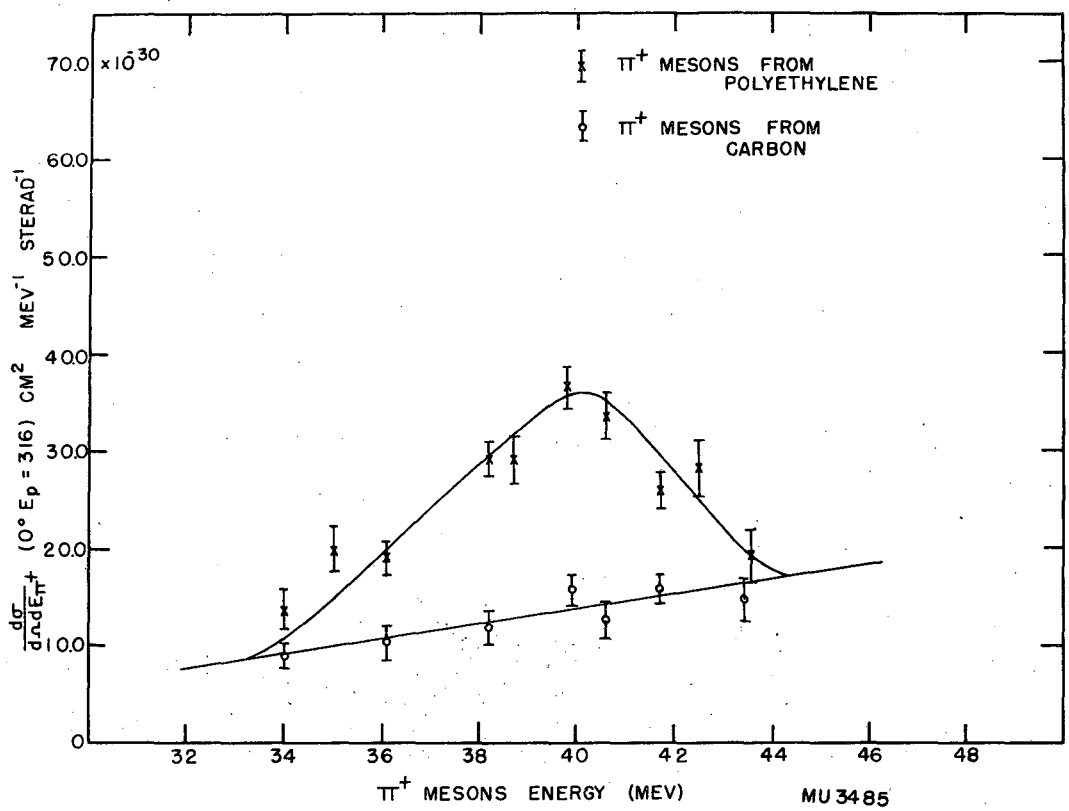
70.0 x10^-30
60.0
50.0
40.0
30.0
20.0
10.0
0
32
34
36
38
40
42
44
46
48
π+ MESONS FROM POLYETHYLENE
π+ MESONS FROM CARBON
dσ/dΩdE_π+ (0° Ep = 316) CM² MEV⁻¹ STERAD⁻¹
π+ MESONS ENERGY (MEV)
MU 3485

Fig. 13

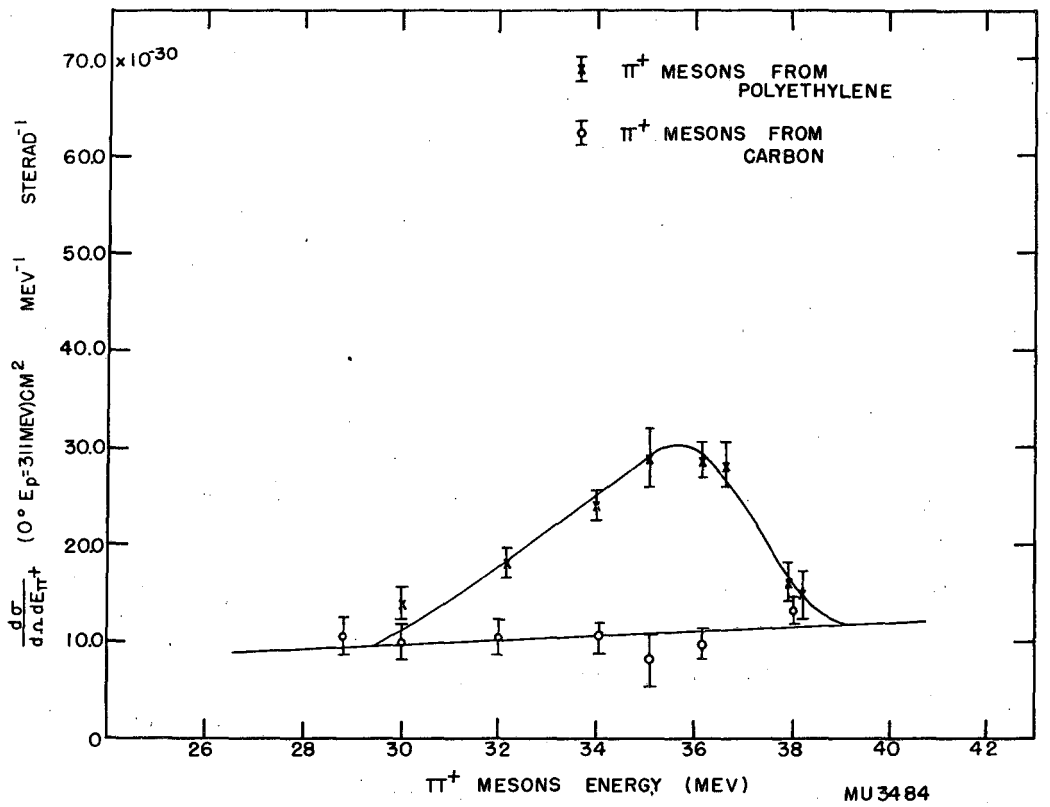
70.0 x10⁻³⁰
60.0
50.0
40.0
30.0
20.0
10.0
0
dσ/dΩ.dE_π+ (0° E_p=311MEV)CM² MEV⁻¹ STERAD⁻¹
π+ MESONS FROM POLYETHYLENE
π+ MESONS FROM CARBON
26
28
30
32
34
36
38
40
42
TT+ MESONS ENERGY (MEV)
MU3484

Fig. 14

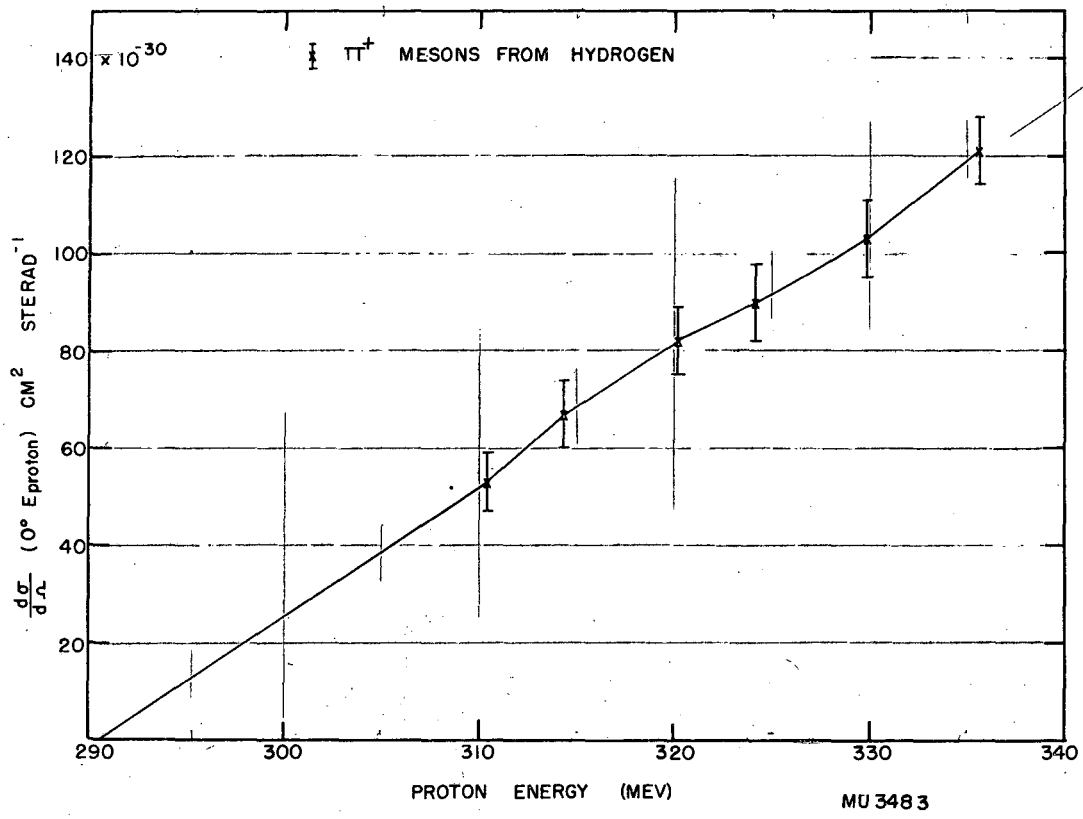
140 x 10^-30
π+ MESONS FROM HYDROGEN
120
100
80
60
40
20
dσ/dΩ (0° Eproton) CM² STERAD⁻¹
290
300
310
320
330
340
PROTON ENERGY (MEV)
MU 3483

Fig. 15

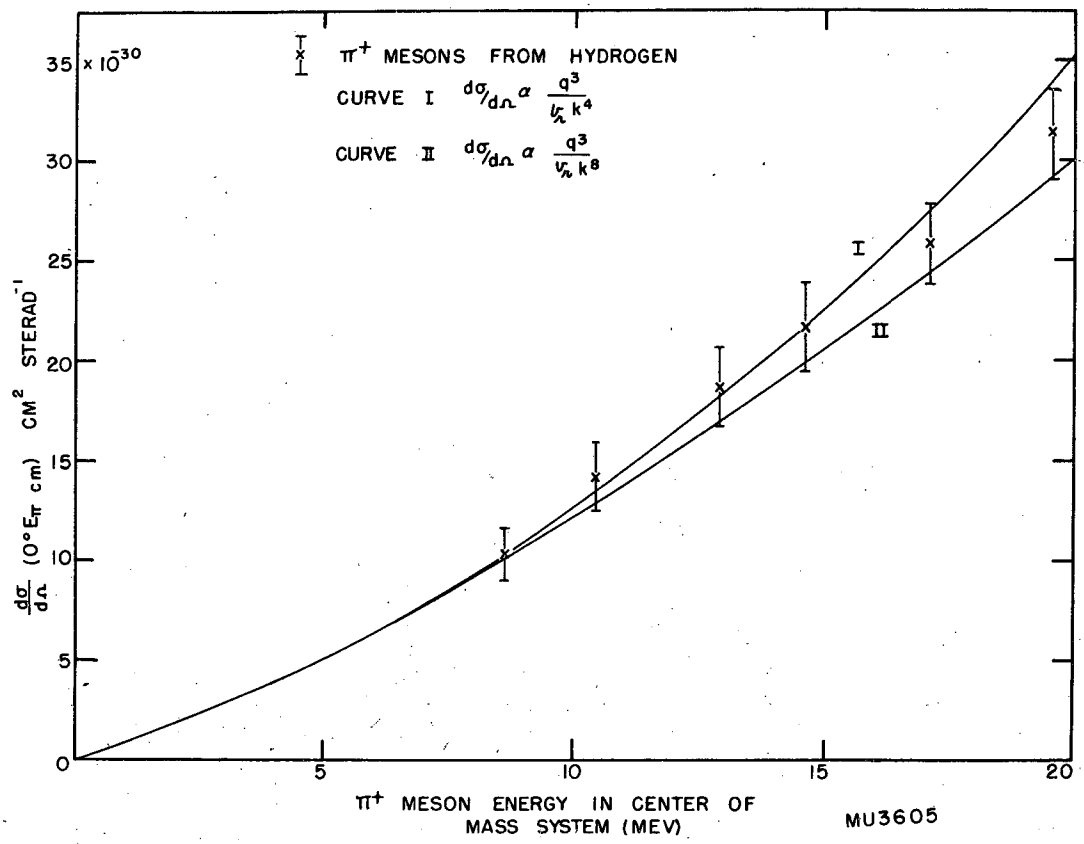
35 x 10⁻³⁰
π⁺ MESONS FROM HYDROGEN
CURVE I dσ/dΩ α q³/ν_π k⁴
CURVE II dσ/dΩ α q³/ν_π k⁸
I
II
dσ/dΩ (0°E_π cm) CM² STERAD⁻¹
0
5
10
15
20
25
30
5
10
15
20
π⁺ MESON ENERGY IN CENTER OF MASS SYSTEM (MEV)
MU3605

Fig. 16

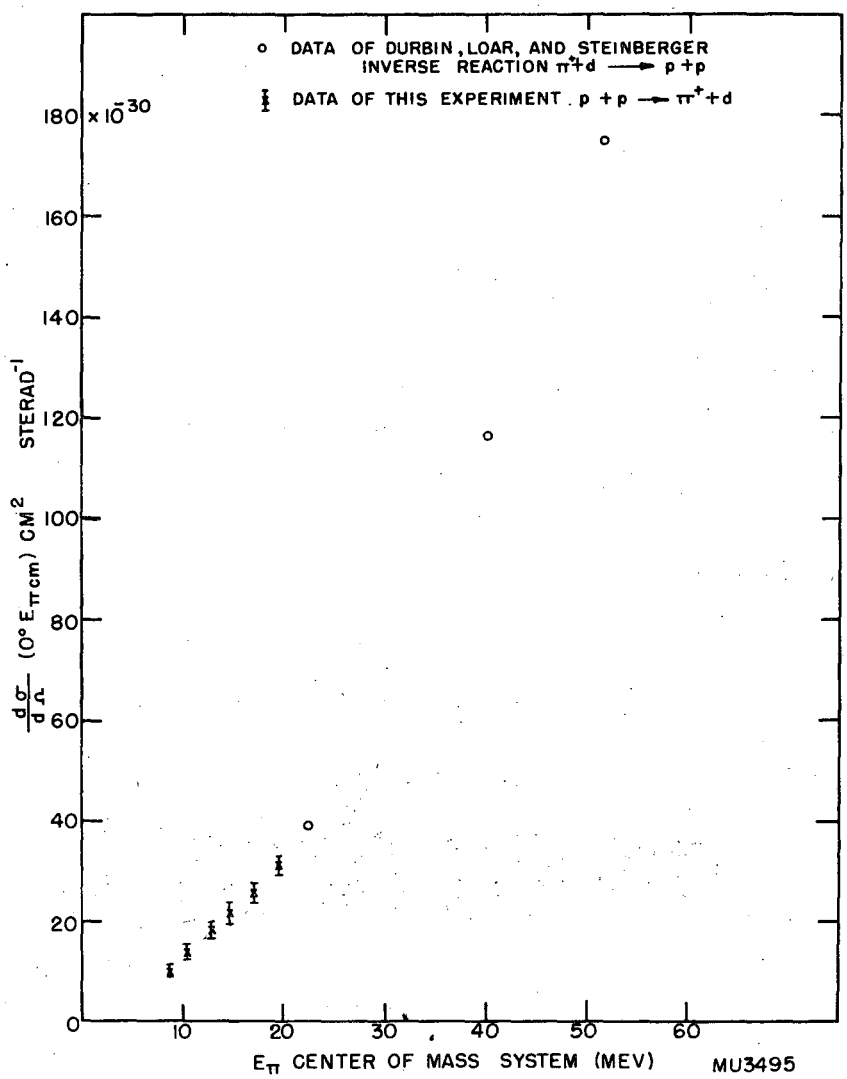
o DATA OF DURBIN, LOAR, AND STEINBERGER
INVERSE REACTION π⁺+d ⟶ p+p
DATA OF THIS EXPERIMENT. p+p ⟶ π⁺+d
180 x 10⁻³⁰
160
140
120
100
80
60
40
20
0
dσ/dΩ (0° Eπcm) CM² STERAD⁻¹
10
20
30
40
50
60
Eπ CENTER OF MASS SYSTEM (MEV)
MU3495

Fig. 17